UNIVERSITY OF OSLO
Department of Geosciences
MetOs section

Impact of ocean heat uptake and release on the climate system during the 20th century

Master thesis in Geosciences; Meteorology and Oceanography

Malin Jeanette Rue

June 16, 2009

Abstract

The heat capacity of the global ocean is very large compared to the rest of the spheres in the climate system of the Earth. It is therefore reasonable to assume that ocean heat uptake or release would manifest itself in corresponding changes in the atmospheric energy content. Since there is no convincing evidence that this is the case, an investigation of this was carried out in this thesis. The archive of IPCC's model runs for the 20th century experiment (20C3M) were used to study the Earth's energy budget by categorizing the main time scales involved and performing separate case studies for each timescale. Four models were evaluated: CCSM3 and Gfdl CM2.0 with variations in both natural and anthropogenic forcing and HadCM3 and Echam5 with only variations in anthropogenic forcing. The results from this thesis showed that the models were relatively realistic regarding the ocean heat content (0-300 m) and global surface air temperature. The ocean and the atmosphere were closely connected, i.e. changes in the ocean usually occurred simultaneously with the atmosphere. Due to major volcanic eruptions occurring in the late 19th and the 20th century, the ocean was rapidly cooled until a recovery was onset over a longer period of time. After the significant increase in greenhouse gases in the middle of the 20th century, there was a clear warming in the ocean in the 1960s, as well as in the atmosphere, in HadCM3 and Echam5. The warming was also evident in CCSM3 and Gfdl CM2.0, but started much earlier due to an increase in incoming solar variability. This warming was anyhow delayed for a couple of decades due to the volcanic eruptions in 1963 and 1982 as well as the increase in anthropogenic aerosols. During the modeled 20th century, cooling events in the climate system were mainly controlled by less energy in the atmosphere, hence in the ocean. Nevertheless, there were occurrences where the ocean provided its own timescale and imposed a cooling signal in the atmosphere, suggesting that the ocean has the ability to independently cool and heat the climate system.

Acknowledgements

First of all I want to thank my supervisor, Cecilie Mauritzen, for great motivation and guidance throughout this whole working process, and for a very interesting topic to work with. And also thanks to Jon Egill Kristjansson for supervision and for proof reading my thesis. I would like to thank Retish Senan for helping me with programming in Ferret, as well as Rasmus Benestad. Thereby I wish to acknowledge use of the Ferret program for analysis and graphics in this thesis (Ferret is a product of NOAA's Pacific Marine Environmental Laboratory, *http://ferret.pmel.noaa.gov/Ferret/*).

Thanks to Gunnar Wollan and Kjell Andresen for helping me with computer problems. Also thanks to Jørn Kristiansen for sharing his knowledge.

I acknowledge the modeling groups, the Program for Climate Model Diagnosis and Intercomparison (PCMDI) and the WCRP's Working Group on Coupled Modelling (WGCM) for their roles in making available the WCRP CMIP3 multimodel dataset. Support of this dataset is provided by the Office of Science, U. S. Department of Energy.

A special thanks to the girls at my study hall for making things a whole lot easier by listening to all my complaints and making jokes to brighten up my day, and for sharing their knowledge. Thank you, Haldis Berge, for proof reading a part of my thesis. Thanks to my family for all the support, and last but not least thanks to Morten for being such a great housewife!

Malin J. Rue, 16.06.2009

Table of Contents

Chapter 1

Introduction

Global heating during the 20th century was caused by a combination of anthropogenic forcing and natural variability. This is verified by the Intergovernmental Panel on Climate Change (IPCC) in a sample of coupled climate model runs. IPCC is a scientific intergovernmental body tasked to evaluate the risk of climate change caused by human activity, and was established in 1988 by the World Meteorological Organization (WMO) and by the United Nations Environment Programme (UNEP). Considering the large heat capacity of the oceans, it is rational to assume that even a small change in ocean heat content, which has been observed on a variety of time and space scales during the 20th century, would manifest itself in corresponding changes in the energy content of the atmosphere. The observed record does not show convincing evidence that this is the case.

By studying the development of Earth's energy budget during the 20th century, even though an accurate calculation can not be performed, we will show that energy fluxes and temperature in the ocean and in the atmosphere are closely connected, and that they fit well with observations. Further on, we will see that ocean heat content follows tropospheric heat content well, and that changes mostly occur first in the atmosphere. By this we mean that the incoming solar radiation is passing through the atmosphere and heating the air first, thereby reaching the ocean. However, some occurrences where the ocean is responsible for a cooling or a warming, will be evident.

We will investigate four models from the sample of IPCC's coupled climate model runs: Ncar CCSM3, Gfdl CM2.0, Ukmo HadCM3 and Mpi Echam5 where we will examine the one dimensional structure (global means) for each variable, i.e. ocean and atmospheric temperatures, energy fluxes, sea ice concentration and water vapor content. The vertical profile development in time (two dimensional) for the temperatures in the atmosphere and in the ocean will also be investigated. In this way it may be possible to see how the ocean heat uptake and release propagates in the rest of the Earth's system. Chapter 2 consists of background and

fundamental information. In chapter 3, models and different methods will be introduced. In section 4.1 a comparison of models to observations will be performed. In section 4.2 we will make a qualitative description of modeled changes in the energy content and in section 4.3 a quantitative analysis of Earth's energy budget, both during the 20th century. In the quantitative analysis there will be three case studies performed: Case 1) Cooling after a volcanic eruption, Case 2) Recovery after a volcanic eruption, and Case 3) Warming due to greenhouse gases. In section 4.4 we will study if a cooling or a warming originates in the ocean. Finally, the conclusions will be revealed in Chapter 5.

Chapter 2

Background

2.1 Earth's energy budget in steady state

We will discuss how radiation is generated in the atmosphere. The energy budget is shown in Figure 2.1 where we have taken the annual and global mean values from Le Treut et al. (2007, IPCC). Shortwave radiation (SW) is radiation emitted

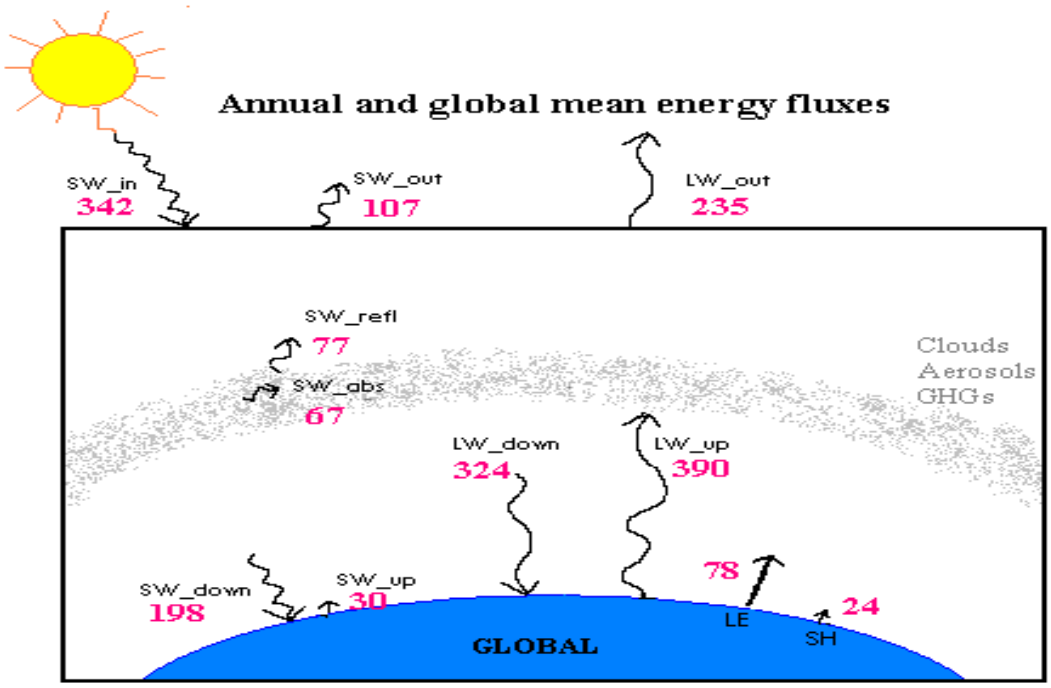

Figure 2.1: *Annual and global mean fluxes taken from Le Treut et al. (2007, IPCC p. 96-97). The unit for the fluxes is W/m*^{2}.

from the sun, and is also referred to as solar radiation. Solar radiation is the driving force of the global climate system and the major energy source for life on Earth. Longwave radiation (LW) is radiation emitted from the Earth, hence also referred to as thermal radiation. Latent heat (LE) and sensible heat (SH) are heat exchanges between the surface and the air above which is a response to turbulence in the boundary layer. The fluxes denoted with underscore down and up are at the surface, while underscore in and out are at the top of the atmosphere. The fluxes have W/m^2 as unit which is how much energy per second (W=J/s) that radiates over an area (m^2). To change the Earth's radiation balance, there must either be a change in the incoming solar radiation; in the amount of solar radiation reflected; or in the longwave radiation reaching the top of the atmosphere (Le Treut et al., 2007, IPCC). To balance the incoming solar radiation from the sun, the Earth has to radiate the same amount of energy back to space. So in a steady state at the top of the atmosphere we have:

$$SW_{in} \;=\; SW_{out} + LW_{out}\;, \tag{2.1}$$

where SW_{in} is the incoming solar radiation and is balanced by shortwave radiation reflected in the atmosphere or at the surface (SW_{out}) and by longwave radiation emitted from the Earth reaching the top of the atmosphere (LW_{out}). The solar radiation absorbed by the Earth is given as (Hartmann, 1994):

$$Absorbed\ solar\ radiation \;=\; S_0(1-\alpha_p)\pi r_p^2\;, \tag{2.2}$$

where S_0 is the solar constant ($S_0 = 1367\ W/m^{-2}$ at a mean distance from the sun to the Earth ($1.5\cdot\ 10^{11}m$)), α_p is the albedo of the Earth's surface, and r_p is the radius of the Earth.

The amount of LW radiation depends on the temperature of the Earth's surface which is derived from the Stefan-Boltzmann's law (Hartmann, 1994):

$$Emitted\ terrestrial\ radiation \;=\; \sigma T_e^4 4\pi r_p^2\;, \tag{2.3}$$

where σ is Stefan-Boltzmann's constant, T_e is the emission temperature and r_p is the same radius as in equation 2.2. When the temperature of the surface increases, the surface will emit more LW radiation. The latter two equations can now be combined since solar radiation absorbed equals planetary radiation emitted, which after some rearrangements results in (Hartmann, 1994):

$$\frac{S_0}{4}(1-\alpha_p) \;=\; \sigma T_e^4 \tag{2.4}$$

From this equation it is possible to compute the emission temperature, T_e, but then we have to keep in mind that equations 2.2 and 2.3 are simplified and that in reality it is more complicated due to many more scattering, reflection and absorption

processes in the atmosphere. But anyhow, this is not a problem in this thesis since we will use radiation and heat fluxes that are already simulated by the models.

The net surface energy balance (F_{net}) averaged over a year is very close to zero, but there are local imbalances, especially over regions of the oceans (Wallace and Hobbs, 2006). At the surface, the net balance includes these fluxes (Wallace and Hobbs, 2006):

$$F_{net} = SW_{down} - SW_{up} + LW_{down} - LW_{up} - LE - SH \ , \tag{2.5}$$

where SW_{down} and SW_{up} are the downwelling and upwelling SW radiation, respectively, and where LW_{down} and LW_{up} are the downwelling and upwelling LW radiation, respectively. LE is the latent heat flux and SH is the sensible heat flux. LW_{down} is a result of absorbed surface emissions of LW radiation, latent and sensible heat transfers, and absorbed SW radiation by gases and clouds emitted from the atmosphere. In Figure 2.1 LW_{up} has the largest value, which is the energy emitted from the Earth's surface. We can see that little SW radiation is reflected at the surface and that the sensible heat flux is just as small, while the SW and LW radiation down at the surface added together, is very large.

SW_{abs} is the shortwave radiation absorbed in the atmosphere before reaching the surface: SW_{abs} = SW_{in} - SW_{down} - SW_{out} + SW_{up}, while SW_{refl} is the shortwave radiation reflected in the atmosphere before reaching the surface: SW_{refl} = SW_{out} - SW_{up}.

Latent heat (LE) is heat transported from e.g. the ocean to the atmosphere through a phase change, like heat loss through melting or evaporation, and is approximately given by the equation from Hartmann (1994):

$$LE = L\rho C_{DE} U_r (q_s - q_a(z_r)) \ , \tag{2.6}$$

where L is the latent heat of vaporization, ρ is the air density, C_{DE} is the aerodynamic transfer coefficient for humidity, U_r is the mean wind at a standard height (z_r), and q_s and $q_a(z_r)$ are the mixing ratios of water vapor at the surface and in the air at z_r, respectively. LE depends on the difference between the moisture at the surface and the moisture at a standard height (z_r) as a response to a difference in the air and water temperatures (or land surface temperature). The ocean is generally a bit warmer than the overlying atmosphere, so if the difference in air and water temperatures increases, i.e. the air temperature above ocean increases more than the sea surface temperature, the evaporation of the surface will increase and hence LE will increase. The evaporation should also increase as the relative humidity decreases or as the wind speed increases. LE is released into the atmosphere when water from the evaporation condenses or freezes.

Sensible heat (SH) is heat exchanged between the ocean surface (or land surface) and atmosphere through conduction or convection across the interface, and

is approximately given by the equation from Hartmann (1994):

$$SH = c_p \rho C_{DH} U_r (T_s - T_a(z_r)) , \tag{2.7}$$

where c_p is the specific heat of air at constant pressure, C_{DH} is the aerodynamic transfer coefficient for temperature, T is the temperature at the surface and at a standard height, z_r, while the other factors are the same as in equation 2.6. SH depends on the difference between air and surface temperature. If the air temperature is colder than the surface temperature, there will be an exchange of heat to the air overlying the surface, hence the word sensible because it is heat we can feel.

2.2 Transformations in the atmosphere

In reality, we know that incoming shortwave (solar) radiation is balanced by longwave (thermal) radiation emitted from the Earth together with heat fluxes (LE and SH). SW radiation acts differently from LW radiation, i.e. they are absorbed differently in their journey through the atmosphere. SW radiation is absorbed by ozone and oxygen molecules in the ultraviolet, by water vapor in the near-infrared (approximately 50% of the solar radiation) and by aerosols in the visible and near-infrared depending on composition and distribution (Jacob (1999); Liou (2002)). The intensity of SW radiation is reduced by absorption, reflection and scattering in its path through the atmosphere by different factors as gases, aerosols and clouds. This can be explained mathematically with a simplified version of the Beer-Lambert-Bouguer law (Wikipedia, 2009):

$$I = I_0 \, e^{-m(\tau_a + \tau_g + \tau_{NO_2} + \tau_w + \tau_{O_3} + \tau_r)} , \tag{2.8}$$

where I is the intensity of the incoming solar radiation after going through the atmosphere, I_0 is the initial intensity, m is the optical mass of the atmosphere and τ is the optical depth (measure of transparency which depends on the absorption coefficient and the density in a layer depth) where a is for aerosols; g is for mixed gases; NO_2 is for nitrogen dioxide; w is for water vapor; O_3 is for ozone; and r is for Rayleigh scattering (O_2, N_2).

LW radiation is absorbed by greenhouse gases: water vapor, carbon dioxide, methane, ozone and various trace gases (Jacob (1999); Liou (2002)). LW radiation is absorbed by low clouds which contain water droplets. The temperature of the low clouds is therefore close to the temperature of the surface due to heat transport by convection. Thus there is only a small greenhouse effect because the low clouds radiate almost the same energy as the surface (Jacob (1999); Liou (2002)). High clouds which contains ice crystals, on the other hand, reflect LW

radiation and induce a net heating because they form an extra layer in the atmosphere , i.e. the greenhouse effect is enhanced (Jacob (1999); Liou (2002)).

Radiative forcing is a measure of how the energy balance of the Earth is affected through altering factors that can influence the climate system, such as greenhouse gases (Forster et al., 2007, IPCC). When the Earth's radiative balance is changed from its normal state, the term forcing can be used.

Greenhouse gases (GHGs) are natural constituents in the atmosphere, but due to anthropogenic activity GHG concentrations may be enhanced (Jacob (1999); Liou (2002)). Water vapor (H_2O) is the most important greenhouse gas because of the large concentration in the atmosphere which is mostly due to the natural source of oceans (Jacob, 1999). H_2O can also provide a strong positive feedback to global warming due to enhanced warming by another greenhouse gas (like CO_2) which results in an increase in H_2O (Jacob, 1999). An increase in water vapor due to this will eventually form clouds which results in precipitation so that the overload of water falls back to the surface and so that the surface temperature does not reach exceedingly high values (Jacob, 1999). Most of the water vapor is concentrated in the lower troposphere, i.e. more than 50% below approximately 850 hPa, so H_2O is of primarly importance to heating in the troposphere (Liou, 2002). Carbon dioxide (CO_2) is also a very important greenhouse gas and because of the long lifetime, CO_2 is equally concentrated in the atmosphere (Liou, 2002). CO_2 has been increasing significant since the late 1950s as a response to the combustion of fossil fuels, absorption and release by the oceans, and photosynthesis (Le Treut et al., 2007; Forster et al., 2007, IPCC). Two other major greenhouse gases, methane (CH_4) and nitrous oxide (N_2O), have increased since 1970 (Le Treut et al., 2007; Forster et al., 2007, IPCC). CH_4 is almost equally distributed in the atmosphere while N_2O has a larger concentration in the stratosphere (Liou, 2002). Synthetic halocarbons, such as chlorofluorocarbons (CFCs), hydrofluorocarbons, perfluorocarbons, halons and sulphur hexafluoride, are also greenhouse gases and have been produced since around year 1930 by the chemical industry (Le Treut et al., 2007, IPCC). These synthetic halocarbons have large global warming potentials. Ozone (O_3) concentrations usually occur approximately between 200 to 20 hPa (stratosphere), and have the largest concentrations around 80 to 40 hPa (Liou, 2002). The stratosphere is cooled by longwave emission from CO_2 and also slightly by H_2O, while O_3 in the stratosphere produce a heating through absorption of solar radiation (Hartmann, 1994, Figure 3.18). In the troposphere, however, a cooling due to longwave emission from CO_2 is approximately balanced by solar absorption by H_2O (Hartmann, 1994, Figure 3.18), and when the surface temperature increases with CO_2 concentration (enhances the total greenhouse effect) the stratosphere cools.

Atmospheric aerosols absorb and scatter solar radiation, and have also indi-

rect effects on cloud cover and cloud albedo, i.e. more aerosols may enhance the cloud cover and cloud albedo depending on size and composition (Hansen et al., 2005). Greenhouse gases on the other hand, absorb and emit longwave radiation which is also the case for large size aerosols (Ramanathan and Feng, 2009). The concentration of aerosols usually decreases rapidly with height in the troposphere (Liou, 2002). Powerful volcanic eruptions, on the other hand, produce aerosols that penetrate up into the lower stratosphere where they have much longer lifetime than in the troposphere because of the lack of precipitation. After a while the volcanic aerosols will fall down to the troposphere where precipitation will carry them further down to the surface (Le Treut et al., 2007, IPCC). Estimates in Stern (2005) show that sulfur emissions have increased in the period of 1850-2000. From around 1930-1940 the global anthropogenic emissions increased rapidly until the early 1980s when a decline in the emissions was evident. The sulfur emissions reached their maximum in year 1989, but have decreased after this (Stern, 2005). From 1961 to 1990 estimates of surface solar radiation have declined by 4% (7 W/m^2) worldwide (Liepert, 2002). An increase in such anthropogenic aerosols which mostly reflect the incoming solar radiation may be the the prime cause of observed "global dimming" (Liepert, 2002) and reduced pan evaporation (Roderick and Farquhar, 2002). Pan evaporation is evaporation from terrestrial water bodies and has been assumed to increase due to an increase in global temperature which makes the air drier and result in more evaporation (Roderick and Farquhar, 2002). Instead the pan evaporation has decreased during the past 50 years which is a consequence of the decrease in solar irradiance and the associated changes in diurnal temperature range and vapor pressure deficit that is observed (Roderick and Farquhar, 2002). Due to greenhouse gases there will be warming which makes the planet wetter, but because of aerosols (anthropogenic and natural), which hinder the solar radiation from reaching the surface, the planet will get drier (Ramanathan and Feng, 2009).

Anthropogenic radiation forcing from greenhouse gases is much larger than natural forcing from solar intensity (Jacob (1999); Liou (2002)).

2.3 On the oceans role in climate

A large part of the change in ocean heat content (OHC) during the past 50 years (1955-2003) occurred in the upper 700 m (Levitus et al., 2005). Levitus et al. (2005) found that the Atlantic Ocean is the biggest contributor to the increase in heat content. Rossby suggested in 1959 that ocean heat content may be the dominant component of the variability of Earth's heat balance compared to other components in the system because of the physical properties and mass of the world

ocean (Levitus et al., 2005). This has been confirmed by Levitus et al. (2005) which estimated that the total increase of heat content of the Earth's system was caused by the oceans by approximately 84% for 1955-1998. Levitus et al. (2005) also mentioned two reasons why they do not expect uniform heating of the ocean from observed increase in greenhouse gases. The first reason was that aerosols can affect the regional warming rates due to variability in concentration geographically. The second reason was that the net heat flux across the air-sea interface regionally would be affected by changes in atmosphere- and ocean circulation due to changes in the Earth's radiative balance. In Levitus et al. (2005) the Earth's heat balance was placed in perspective, and the response of Earth's climate system to changes in radiative forcing is often due to how the surface temperature respond to the radiative forcing. This is simply because there has been a scarcity of subsurface ocean data to combine with Earth system heat balance studies. Levitus et al. (2005) concluded that there has to be an improved scientific understanding which requires studying of the response of all components of the Earth's heat balance, where the world ocean is the dominant term.

The thermohaline circulation is a large-scale ocean circulation that is driven by global density gradients created by surface heat and freshwater fluxes. Warm, saline water in the surface layer is transported northward into the North Atlantic where it cools and sinks down to form deep water. The deep water formed in the North Atlantic is then transported southward to join the current in the Southern Ocean. From the Southern Ocean the deep water circulation enters the Pacific and Indian Oceans. The thermohaline circulation warms the climate in Europe through the supply of warm waters from the south. Abrupt changes in the circulation pattern which result in dramatic climate responses are limited mainly to the North Atlantic (Broecker, 1997). A large increase of greenhouse gases could lead to a collapse of thermohaline circulation through warming and freshening of polar waters (Broecker, 1997). Up to the end of the 20th century the thermohaline circulation has probably been changing significantly at interannual to decadal time scales, but however, there are no coherent evidence found for a trend in the mean strength of the circulation because of uncertainties in the observational record (Bindoff et al., 2007, IPCC).

The IPCC report (Bindoff et al., 2007, IPCC) states that the oceans are warming, and for the 0-700 m layer global ocean temperature rose by 0.10° for the period 1963 to 2003. During the same period global ocean heat content (0-3000 m) increased equivalent to the globally averaged absorbing energy (0.21 ± 0.04 W/m^2).

Chapter 3

Methods

3.1 Models

We will use the archive of IPCC's model runs for 'Climate of the 20th century experiment' (20C3M) from the World Climate Research Programme's (WCRP) Coupled Model Intercomparison Project 3 (CMIP3) multi-model dataset to investigate Earth's energy budget. The Program for Climate Model Diagnosis and Intercomparison (PCMDI) made these model outputs available via the Earth System Grid (ESG) data portal[1]. The WCRP CMIP3 multi-model database is meant to serve IPCC's Working Group 1, which focuses on the physical climate system, and the choice of variables archived at the PCMDI reflects this focus. The PCMDI mission is to develop improved methods and tools for the diagnosis and intercomparison of multiple coupled ocean-atmosphere general circulation models (GCMs) that simulate the global climate.

We will assess the mean state and time variability of energy content in the ocean and in the atmosphere, and investigate what happens when the oceans release or take up significant amounts of heat and how it propagates in the rest of the Earth's system. The work involves categorizing the main time scales involved and performing separate case studies for each timescale. We will examine global means throughout the text. Four models are evaluated:

1. Community Climate System Model, version 3 (CCSM3) - National Center for Atmospheric Research, USA (2005)

2. Coupled Climate Model 2.0 (CM2.0) - National Oceanic and Atmospheric Administration's (NOAA) Geophysical Fluid Dynamics Laboratory (GFDL), USA (2004)

[1]Model outputs can be downloaded on request from a catalogue of the IPCC sampling of climate model runs on *https://esg.llnl.gov:8443/*.

3. Hadley Centre Coupled Model, version 3 (HadCM3) - Hadley Centre for Climate Prediction and Research/Met Office, UK (1997)

4. European Centre Hamburg Model, version 5 (Echam5) - Max Planck Institute Meteorology, Germany (2005)

The reason for using CCSM3 is because this model is in use at the Department of Geosciences, and HadCM3 was chosen because it has been analyzed extensively with respect to the freshwater-exchanges in the North Atlantic. The models were, besides this, randomly selected from the models available on WCRP CMIP3 Multi-Model Database where we could choose from 25 different models.

All the flux variables that we use are simulated with the presence of clouds, and we get them from the WCRP CMIP3 Multi-Model Database mentioned at first. In all the data sets the grid points are interpolated, i.e. new grid points are constructed within a range of a discrete set of known grid points. For the models we use monthly data from Run 1, because of the widest selection of variables. The variables, which we will examine, are listed below.

1. Ocean
    - Potential temperature down to 2000 m
    - Heat content in 0-300 m (modeled and observed)
2. Atmosphere
    - Air temperature in all levels
    - Heat content in 1000-200 hPa (troposphere) and 200-10 hPa (stratosphere)
    - Surface temperature (modeled and observed)
    - Water vapor content
3. Radiation - at the top of the atmosphere and at the ocean surface
    - Shortwave
    - Longwave
4. Sensible and Latent heat fluxes at the ocean surface
5. Cryosphere
    - Sea Ice Concentration

All the models are coupled climate models. In every model the pressure levels in the atmosphere are given from 1000 hPa to 10 hPa, but the number of levels varies from model to model (see Table 3.1), also in depth levels. CCSM3 and Gfdl CM2.0 have both variations in natural and anthropogenic forcings during the 20th century, while HadCM3 and Echam5 only have variations in the anthropogenic forcings (see Table 3.2). Model simulations are based on variations in the long-lived greenhouse gases (LLGHG's) that are reasonably constrained by the observational record (Meehl et al., 2007, IPCC). In Figure 3.1 (Forster et al., 2007, IPCC Fig.2.23), the radiative forcing is simulated for the Model for Interdisciplinary Research on Climate (MIROC) + Spectral Radiation-Transport Model for Aerosol Species (SPRINTARS) general circulation model due to various agents. The greenhouse gas increase is present during the whole period of time, but there is an even more significant increase from around year 1950 and since this figure applies to most models regarding the evolution of the LLGHG's radiative forcing, we assume that this applies to our models as well since they are a part of the IPCC's model runs for 'Climate of the 20th century experiment'.

HadCM3 has the crudest resolution and CCSM3 has the finest resolution as shown in Table 3.1. Even though Echam5 is run for the period 1860-2009, we will only study the period 1860-1999 as for HadCM3.

Atmosphere			
Model	**Resolution (Lon x Lat)**	**Levels**	**Period of model run (years)**
CCSM3	256x128 (1.4°x1.4°)	17	1870-1999
Gfdl CM2.0	144x90 (2.5°x2.0°)	17	1861-2000
HadCM3	96x73 (3.75°x2.5°)	15	1860-1999
Echam5	192x96 (1.88°x1.88°)	16	1860-2009
Ocean			
Model	**Resolution (Lon x Lat)**	**Levels**	**Max depth (m)**
CCSM3	320x395 (1.1°x0.5°)	40	5375
Gfdl CM2.0	360x200 (1.0°x0.9°)	50	5316
HadCM3	288x144 (1.25°x1.25°)	20	5192
Echam5	360x180 (1.0°x1.0°)	40	5720

Table 3.1: *Model properties.*

Volcanic forcing is a natural forcing which is only included in CCSM3 and Gfdl CM2.0, and not in HadCM3 and Echam5. Because of this CCSM3 and Gfdl CM2.0 will be referred to as the volcanic models (V-models) and HadCM3 and Echam5 the non-volcanic models (non-V models). The V-models have also

variations in the solar forcing which the non-V models do not have, i.e. an increase in the incoming shortwave radiation.

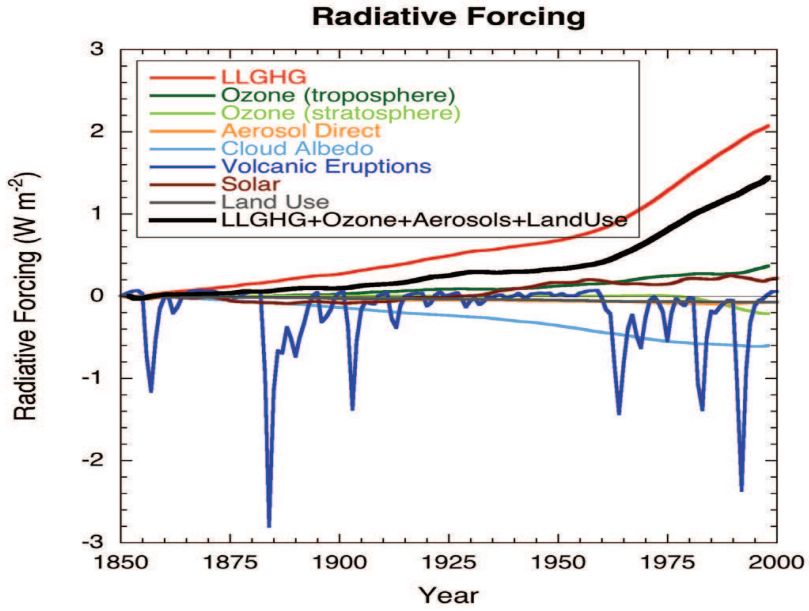

Figure 2.23. *Globally and annually averaged temporal evolution of the instantaneous all-sky RF (top panel) and surface forcing (bottom panel) due to various agents, as simulated in the MIROC+SPRINTARS model (Nozawa et al., 2005; Takemura et al., 2005). This is an illustrative example of the forcings as implemented and computed in one of the climate models participating in the AR4. Note that there could be differences in the RFs among models. Most models simulate roughly similar evolution of the LLGHGs' RF.*

Figure 3.1: *Figure 2.23 from IPCC (Forster et al., 2007).*

Model	G	O	SD	SI	BC	OC	LU	SO	VL
CCSM3	Y	Y	Y	-	Y	-	-	Y	Y
Gfdl CM2.0	Y	Y	Y	-	Y	Y	Y	Y	Y
HadCM3	Y	Y	Y	Y	-	-	-	-	-
Echam5	Y	Y	Y	Y	-	-	-	-	-

Table 3.2: *Forcing agents in IPCC's climate of the 20th century experiment (Santer et al., 2007, SI Table 2). G=Well-mixed greenhouse gases; O=Tropospheric and stratospheric ozone; SD=Sulfate aerosol direct effect; SI=Sulfate aerosol indirect effect; BC=Black carbon; OC=Organic carbon; LU=Land use change; SO=Solar irradiance; and VL=Volcanic aerosols. Mineral dust and sea salt are not included in the models.*

In Table 3.2 are all the forcing agents for each model in IPCC's 20th century experiment listed. All the models have variations in well-mixed greenhouse gases, in tropospheric and stratospheric ozone, and in the sulphate aerosol direct effect. The latter means that the incoming solar radiation is relfected. The sulphate aerosol indirect effect means that the aerosols alter the cloud cover and the cloud albedo, and is only included in the non-V models. CCSM3 and Gfdl CM2.0 have the same forcings, but in addition Gfdl CM2.0 includes organic carbon and land use change. HadCM3 and Echam5 have all the same forcings.

3.2 Theory

In an ideal system we should be able to follow the energy from the sun as it distributes itself into the atmosphere, land, cryosphere and ocean, and eventually back to space. In practice, the models contain numerous parameters and approximations such that calculating a heat budget for the Earth will not be accurate. Nevertheless, we will derive an expression for the heat content of the atmosphere and of the ocean to evaluate the heat budget of the Earth.

3.2.1 Atmospheric heat content equation

The potential and internal energy are not independent forms of energy in the atmosphere (Peixoto and Oort, 1992). If we assume that the atmosphere is in hydrostatic equilibrium, then the potential and internal energy are proportional to each other. Because of this it is practical to consider them together as one form of energy: the total potential energy. The pressure-integrated form of the equation for the total potential energy in an atmospheric column from Peixoto and Oort (1992) is:

$$\int_0^\infty \rho \, (\Phi + I) \, dz = \int_0^p c_{p_a} \, T \, \frac{dp}{g}, \tag{3.1}$$

where c_{p_a} is the specific heat capacity for dry air at constant pressure (1004 $J/(K \cdot kg)$), T is the air temperature at a given pressure level (dp), and g is the gravitational acceleration (9.81 m/s^2). Φ is the potential energy and I is the internal energy given as:

$$\begin{aligned} \Phi &= gz \, , \\ I &= c_v T \, , \end{aligned} \tag{3.2}$$

where g is the gravitational acceleration, z is the height, c_v is the specific heat capacity for dry air at constant volume and T is the temperature. Equation 3.1 only

gives us the energy for a unit column. To get the equation for the global atmospheric heat content, we need to integrate over the area. Since we are dealing with latitude and longitude in our model datasets, we have to find a way to compute the area for each grid point. We use the definition of an increment of the solid angle (Hartmann, 1994):

$$d\omega \;=\; sin\theta \; d\theta \; d\phi, \tag{3.3}$$

where θ is the latitude (zenith angle) and ϕ is the longitude (azimuth angle). This equation is the angle from the Earth's crust to the surface between a certain latitude and longitude which forms an area at the Earth's surface. We have to multiply the solid angle with the square of Earth's radius to get the area:

$$dA \;=\; R^2 \cdot d\omega \;=\; R^2 \sin\theta \; d\theta \; d\phi \tag{3.4}$$

From equation 3.1 we can compute the global atmospheric heat content by multiplying with the area (dA) from equation 3.4:

$$AHC_{monthly} \;=\; \int_{\phi_1}^{\phi_2} \int_{\theta_1}^{\theta_2} \int_{p_2}^{p_1} c_{p_a} \, R^2 \, T \, \frac{dp}{g} sin\theta \; d\theta d\phi, \tag{3.5}$$

where *AHC* stands for atmospheric heat content and is a volume integrated measure of the air temperature.

3.2.2 Ocean heat content equation

The equation for ocean heat content is derived from the conservation law of heat (Mauritzen, 1996):

$$\frac{\partial \rho \Theta}{\partial t} \;+\; \nabla \cdot \; \rho \Theta \vec{u} \;=\; 0, \tag{3.6}$$

where ρ is the density; Θ is the potential temperature; and $\vec{u}$ is the velocity-vector. The ∇-operator term is the advection term in flux form, while the other term is the time evolution term. Since we look at the ocean globally, the advection term is neglected. The only exchanges of heat are then through the air-sea fluxes, i.e. the surface energy balance (F_{net}), which is given in equation 2.5. Fluxes that point down toward the surface are positive since the surface gains energy, while fluxes that point up from the surface are negative (LW_{up}, LE and SH points up) since the surface loses energy to the atmosphere. Figure 3.2 illustrates how volume transport and air-sea fluxes (here called Q_{in} and Q_{out} as in "net energy in" and "net energy out") act in a water column.

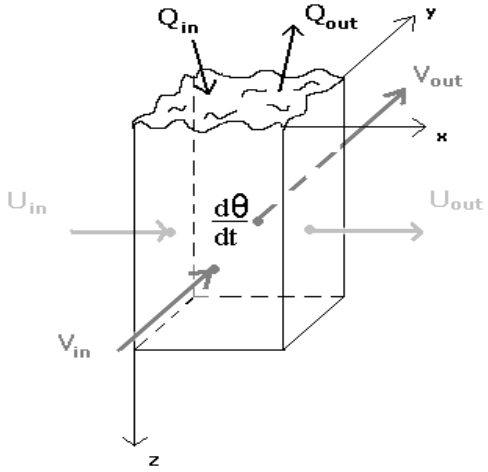

Figure 3.2: *U and V are the volume transports in and out of the column; Q_{in} is the sum of surface fluxes down at the interface (SW_{down}-SW_{up}+LW_{down}) and Q_{up} is the sum of surface fluxes up from the interface (LW_{up}+LE+SH); $\frac{d\Theta}{dt}$ is the time changing potential temperature of the water column. The z-axis is positive downwards.*

The final equation for ocean heat content is then (Mauritzen, 1996):

$$H = \int \rho c_p \Theta dz, \tag{3.7}$$

which is the heat content (Joule) per square meter. To get the global ocean heat content (Joule) the same method as for global atmospheric heat content has to be used, i.e. we integrate over the area $dA = dxdy$:

$$OHC = c_{p_o}\, \bar{\rho}\, \Theta\, dxdydz, \tag{3.8}$$

where *OHC* stands for ocean heat content and is a volume integrated measure of the ocean temperature. Θ is the potential temperature depending on position (x,y,z); $dxdy$ is the area for each grid point (dA); dz is the depth interval; $\bar{\rho}$ is the average sea water density (1025 kg/m^3); c_{p_o} is the specific heat capacity for water at constant pressure ($4.0 \cdot 10^3\ J/(K \cdot kg)$). We have chosen the density as a constant since changes in global averaged density throughout the 20th century are small compared to changes in the global averaged temperature. Inserting for dA from equation 3.4 we get:

$$OHC_{monthly} = \int_{\phi_1}^{\phi_2} \int_{\theta_1}^{\theta_2} \int_{0}^{Z} c_{p_o}\, \bar{\rho}\, R^2\, \Theta\, sin\theta\, dz d\theta d\phi, \tag{3.9}$$

where Θ now depends on the position of latitude (θ), longitude (ϕ) and depth (z).

3.3 Making the plots

In the previous section we showed how to calculate the atmospheric and ocean heat contents, but in this thesis we will simply do all the calculations in Ferret (explained under) and plot them directly (Ferret is a free data visualization and analysis program, and can be downloaded on *http://ferret.pmel.noaa.gov/Ferret/home*). We will examine the climatology for all the variables, i.e. we make plots of the anomalies by subtracting the mean value found for each month (January, February, etc., in the selected period of time) from the monthly values. In this way a change during the 20th century in e.g. the energy fluxes can be more easily investigated since the actual values are so different in size as shown in Figure 2.1 (section 2.1).

To compute the ocean heat content, we use the transformation @DIN in Ferret which is the definite integral. @DIN is used for the x, y and z coordinates of the potential temperature, i.e. the latitude, the longitude and the depth position. When @DIN is applied simultaneously to both the x and y axes (in units of degrees of longitude and latitude, respectively) the calculation will be carried out on a per-unit-area basis (as a true double integral). This ensures that the COSINE (latitude) factors will be applied correctly. The same applies to @AVE simultaneously on x and y (used in the computations for global averages). So the transformation first computes the definite integral in one grid point to get the area and then the definite integral for a depth interval (dz) we have chosen in the same grid point, to get the volume integrated potential temperature in that grid point. The integration continues to the next grid point and does the same computation for every grid point. Finally, it sums up all the values for each grid point and multiplies them with the heat capacity for water (c_{p_o}) and the average sea water density to get the total heat content of the ocean (see equation (3.9)). This method is also used to compute the atmospheric heat content, but instead with equation 3.5 where we use @DIN on the air temperature (T) for a pressure interval (dp) and multiply with c_{p_a}/g in the end.

A contour plot of the temperature in the ocean and in the atmosphere, i.e. the temperature for each level, is made by computing the anomalies for each level of the ocean and the atmosphere. The result is a timedeveloping contour plot of the temperature shown in section 4.2.

We use a land sea mask file[2] to obtain values over ocean or over land only. This varies from model to model, but mostly the values for ocean are set to zero while for land they are set to one or the percentage of land. Ocean-values are then given by multiplication of one minus the land sea mask file and the variable. Then values equal to zero, which is for land, are removed to get exact means for the ocean values. For land, the variable is multiplied with the land sea mask file so that ocean-values are set to zero. In this way we can see how air temperature and radiation vary over ocean or over land. We will in this thesis mainly focus on the values over ocean.

All the plots are anomalies if not otherwise mentioned, and they are all 5-year filtered (60 time point filter in Ferret) except for Figure 4.1 and 4.2 where we use 3-year filtering, because Domingues et al. (2008) use this for the observations of ocean heat content which we will compare with later. The observations used from NASA (2009) and HadCRU (Jones and Salmon, 2008) are yearly means where information on filtering was not available.

[2]Download from:
http://www.ipcc-data.org/ar4/model-GFDL-CM2-change.html for Gfdl CM2.0
http://www.ipcc-data.org/ar4/model-UKMO-HADCM3-change.html for HadCM3
http://www.ipcc-data.org/ar4/model-MPIM-ECHAM5-change.html for Echam5
(accessed January 2009)
The land-sea mask file for CCSM3 was obtained from outputs from the European Centre for Medium-Range Weather Forecasts (ECMWF) operational analysis and forecasting system on *http://www.ecmwf.int/products/data/operational_system/index.html*.
(accessed from Retish Senan (Norwegian Meteorological Institute) January 2009)

Chapter 4

Results and discussion

In this chapter, the different models will be investigated and the one dimensional structure for each variable (global means) will be examined. In this way it may be possible to see how the ocean heat uptake and release propagate in the rest of the Earth's system. We start by comparing the models with observations to check if the models are reliable. We will then make a qualitative description of modeled changes in the energy content during the 20th century, and then a quantitative analysis of Earth's energy budget during the 20th century. In the quantitative analysis we will do three case studies: Case 1) Cooling after a volcanic eruption, Case 2) Recovery after a volcanic eruption, and Case 3) Warming due to greenhouse gases. In section 4.4 there will be studied if a cooling or a warming originates in the ocean.

4.1 Comparing models with observations

We will compare each model with observations for ocean heat content, global air temperature and land air temperature. The ocean heat content observations were obtained from CSIRO[1] Climate Marine and Atmospheric Research[2] (Domingues et al., 2008) to compare with our modeled ocean heat content. To compare the modeled surface air temperature, we use the global-mean annual values for surface air temperature from NASA (2009) and HadCRUT3 (Jones and Salmon, 2008). We also use land means (CRUTEM3 from Jones and Salmon (2008)) to compare with modeled surface air temperature just over land. The reason for doing this is to investigate if it is due to the lack of observations over oceans that there are some deviations in the global means.

[1] Commonwealth Scientific and Industrial Research Organization

[2] The data may be downloaded on request from *http://www.cmar.csiro.au/sealevel/sl_data_cmar.html* (accessed February 2009).

By comparing the models with observations we establish how realistic the four models are. We will also see how models with or without volcanic forcing compare to the observations. The observation data for ocean heat content (Domingues et al., 2008) is given in 0-300 m, and only for 1950-1999. So we can only compare the period 1950-1999 for the ocean heat content, while for the surface air temperature we have observations from 1880 to 1999.

4.1.1 Ocean heat content

We begin by comparing the models that include volcanic forcing to the observations for ocean heat content. In the period of observations (1950-1999) there are three major volcanic eruptions: Agung (Bali) in 1963, El Chichon (Mexico) in 1982 and Pinatubo (the Philippines) in 1991 (from Figure 8.13 in Liou (2002)). Out of these three eruptions, Pinatubo is most powerful. Major volcanic eruptions can cause a short-lived (2-3 years) negative forcing through the temporary increases of sulphate aerosols in the stratosphere (Forster et al., 2007). Figure 4.1 and 4.2 show ocean heat content anomalies computed from 1950-1999 means, while the observations from Domingues et al. (2008) are relative to year 1961. This can be done since it is only the variations and the development of the ocean heat content we are investigating. And by doing this, the comparison will be simpler to investigate since we choose where we want the zero-crossing to be.

From Figure 4.1 it is obvious that CCSM3 fits better with the observations than Gfdl CM2.0. At the starting point, both CCSM3 (black curve) and Gfdl CM2.0 (green curve) have almost the same value as the observations (pink curve), and they are very close to the observations until around 1965. From 1965 to 1975, neither V-model follows the observations very well. It is evident that a recovery after the Agung eruption (1963) in the modeled ocean heat content (Figure 4.1) occurs a few years earlier than for the observations, i.e. from around 1965. In the period of 1965-1975, the V-models do not deviate in the same way as the observations do. The El Chichon eruption (1982) results in a quite strong cooling for Gfdl CM2.0, while for CCSM3 and the observations the cooling is not so significant. CCSM3, along with the observations, have a greater increase than Gfdl CM2.0 after 1975. Despite this, they both deviate in the same way due to the three volcanic eruptions in 1963, 1982 and 1991.

The non-V models in Figure 4.2 do not fit as well with the observations as the V-models do from 1950 to around 1965-1970, but they do follow the observations quite closely from around 1965-1970 throughout the 20th century. Echam5 is a bit closer to the observations in the beginning, but after 1985 HadCM3 is closer to the observations. As was obvious, both HadCM3 and Echam5 are very close to the observations after 1970, but they do not reproduce the decadal variations which are evident in the observations and for the V-models (Figure 4.1) in this

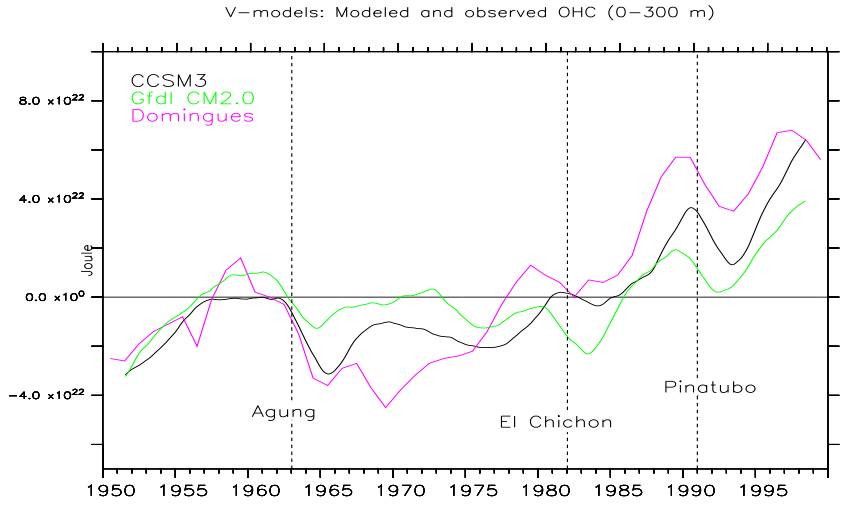

Figure 4.1: *V-models: Ocean heat content anomalies compared with observations (Domingues et al., 2008). The modeled anomalies are computed from 1950-1999 means, while the observations are relative to year 1961(zero-crossing).*

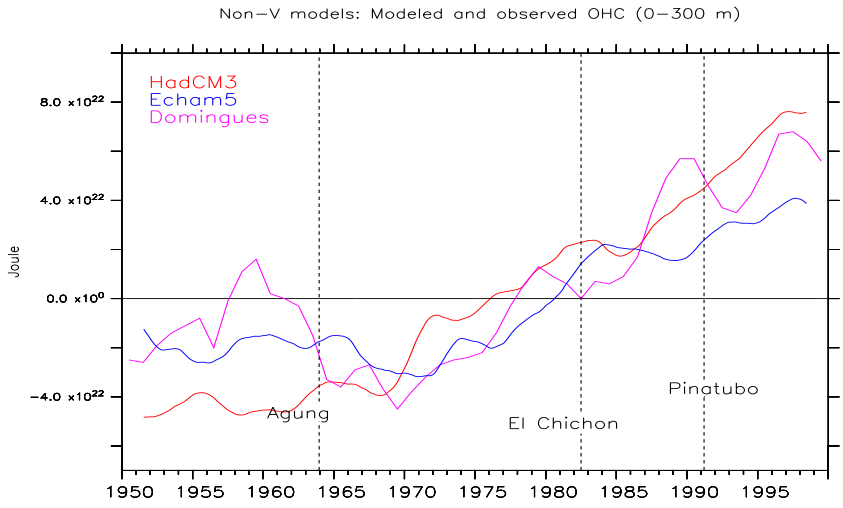

Figure 4.2: *Non-V models: Ocean heat content anomalies compared with observations (Domingues et al., 2008). The modeled anomalies are computed from 1950-1999 means, while the observations are relative to year 1961(zero-crossing).*

period.

With no volcanic forcing in the models (non-V models), the significant peak in 1950 to 1965 in the observations is not there, and the models are closer to the

observations after approximately 1965, and even closer than the models with volcanic forcing, especially in the period 1965 to 1975. But remember that the non-V models do not reproduce the decadal variations. Cooling from the Agung eruption (1963) in the V-models is smaller and lasts shorter compared to the observations. It then seems like the V-models do not have as strong volcanic forcing as the observations indicate to entirely reproduce the significant cooling evident in the observations. But this can also be in connection with that there was a large amount of anthropogenic aerosols available around these times which also contribute to cooling.

In climate models with volcanic forcing, the decadal variability agrees approximately with the observations, but the observed multi-decadal trends are greater than the modeled trends (Domingues et al., 2008). Domingues et al. (2008) show from 1961 to 1999 that the trends in volcanic models are closer to the observations, but that the heat storage is only 73% in 0-300 m for the models compared to 93% in the observations. From the experience of comparing models to observations, we found that the models with volcanic forcing reproduced the ocean heat content better than the non-V models almost during the whole period of time. But overall, both V-models and non-V models are quite close to the observations of ocean heat content, especially in the period after approximately 1970.

4.1.2 Global surface air temperature

We show in Figure 4.3(a) the global surface air temperature for the four models and two datasets of observations (NASA (2009) and HadCRUT3 from Jones and Salmon (2008)). The reason for picking two datasets of observations is simply to check if there are large differences in the observations. The observation anomalies from NASA (2009) are relative to 1951-1980 means, and the HadCRUT3-anomalies are relative to 1961-1990. We can see that the two observation curves are quite close, but that the HadCRUT3 observations (Jones and Salmon, 2008) have larger negative deviations so that the models are closer to the observations from NASA (2009). This is just due to where they set the zero-crossing because the variations for HadCRUT3 are evident in all the models. From the beginning (1880), CCSM3 and Gfdl CM2.0 (V-models) follow the observations all the way to the late 1940s. After this there is a significant peak in the V-models that lasts from approximately 1950 to 1965 which is not obvious for the observations or for HadCM3 and Echam5. From the beginning to around 1930 the non-V models have smaller deviations than the observations and the V-models, so until 1930 the V-models reproduce the global surface temperature best. After 1930-1940 the non-V models follow the observations quite well throughout the century, while the V-models have a significant peak from approximately 1950 to 1965 which is not evident in the observations. Despite these differences, all the models are very

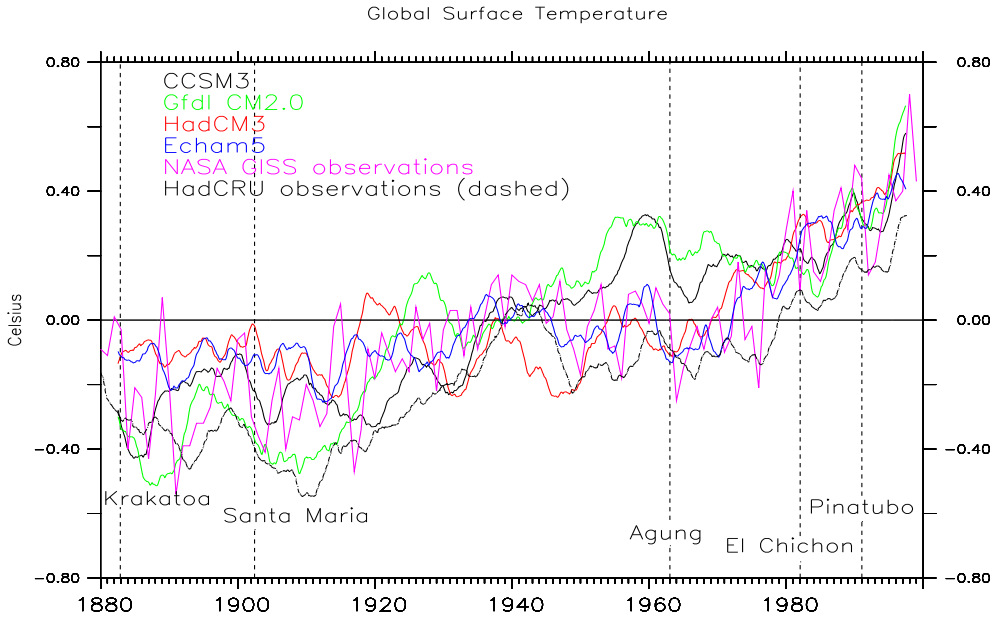

(a) Global

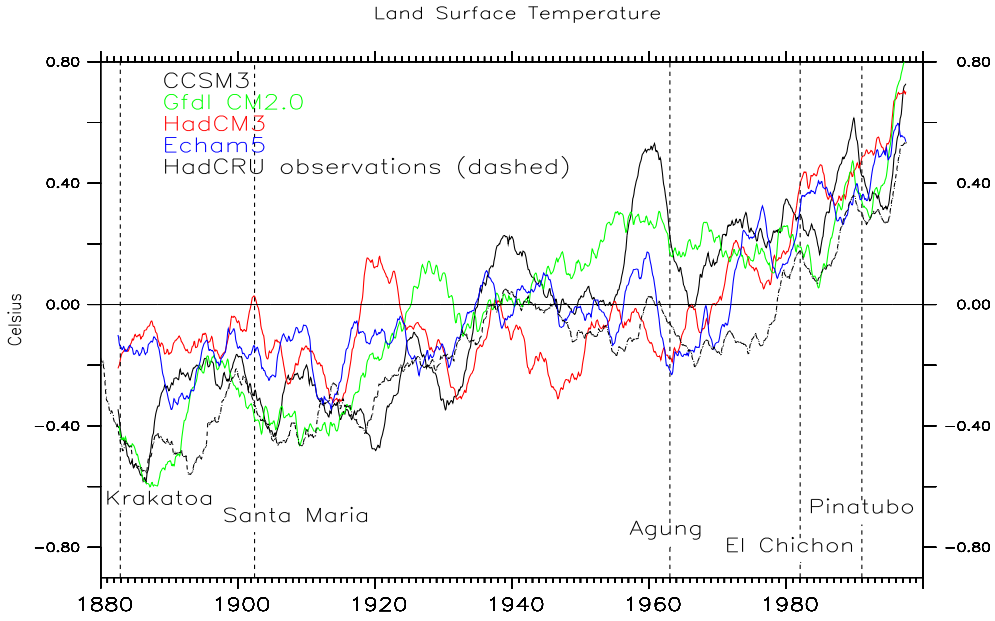

(b) Land

Figure 4.3: *Global and land surface air temperature anomalies for the models and observations (NASA (2009); HadCRUT3 and CRUTEM3 from Jones and Salmon (2008)). The anomaly values given from NASA (2009) are calculated from 1951-1980 means and from Jones and Salmon (2008) they are calculated from 1961-1990 means, while the modeled anomalies are relative to 1880-1999.*

close to the observations from the late 1970s to 1999, and they are even closer than before.

In Figure 4.3(b) we have made a plot of the land values for surface air temperature for the four models and for the CRUTEM3 observations (Jones and Salmon, 2008). The reason for doing this is because of the significant peak that was evident for the V-models from approximately 1950 to 1965 in Figure 4.3(a). This can be due to the lack of observations over ocean which is a great hindrance in research or it can be due to the various inputs in the models. The V-models follow the observations best in the beginning until around 1940 in Figure 4.3(b), while the non-V models are not that close which was also obvious in Figure 4.3(a). From approximately 1950 to 1965 the significant peak is still obvious for CCSM3 and Gfdl CM2.0, also for Echam5, while HadCM3 actually compares best to the observations. After this period, they are all very close to the observations as in Figure 4.3(a). By studying the land surface air temperature for the models with observations, we find that the significant peak from approximately 1950 to 1965 is still only visible in the models (except for HadCM3) and not in the observations. As we saw in section 4.1.1, the V-models were closer to the observations from 1950 to 1965 than the non-V models for the ocean heat content, while here the non-V models are closer to the observations than the V-models for surface air temperature, both global and land.

4.1.3 Vertical temperature profiles

We will now examine modeled vertical temperature profiles of the atmosphere and ocean to see how realistic they are. We choose at random the modeled mean values of year 1960 for the vertical temperatures shown in Figure 4.4 (there are no significant changes in the globally averaged vertical profile for each model during the 20th century). In the troposphere the temperature decreases with height while in the stratosphere there is an isotherm layer from around 300-200 hPa to 100 hPa and above this the temperature increases. The tropopause is the segregation between the troposphere and the stratosphere and is approximately at 300-200 hPa (global average), differing from latitude to latitude (see Figure 3.1 in Liou (2002)). The temperature decrease with height in the troposphere is determined by the radiative balance and the convective transport of energy from the surface to the atmosphere (Liou, 2002). Water vapor, clouds and precipitation are confined to the troposphere and contribute to the temperature distribution (Liou, 2002). The temperature increase in the stratosphere is primarily determined by the absorption of solar radiation by ozone and through the emission of infrared fluxes by carbon dioxide (Liou, 2002).

In Figure 4.4(a) the temperature profiles of the models are quite similar. Gfdl CM2.0 is 2-3 °C colder than the other three in the troposphere. From 1000 to 930

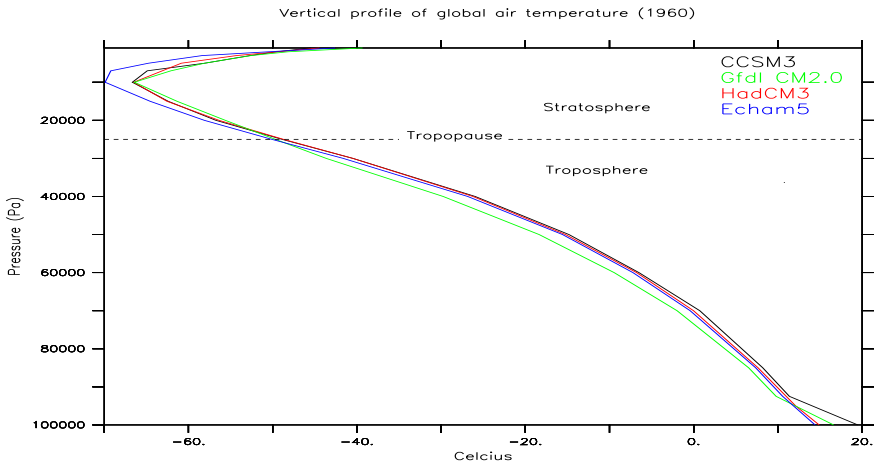

(a) Atmosphere

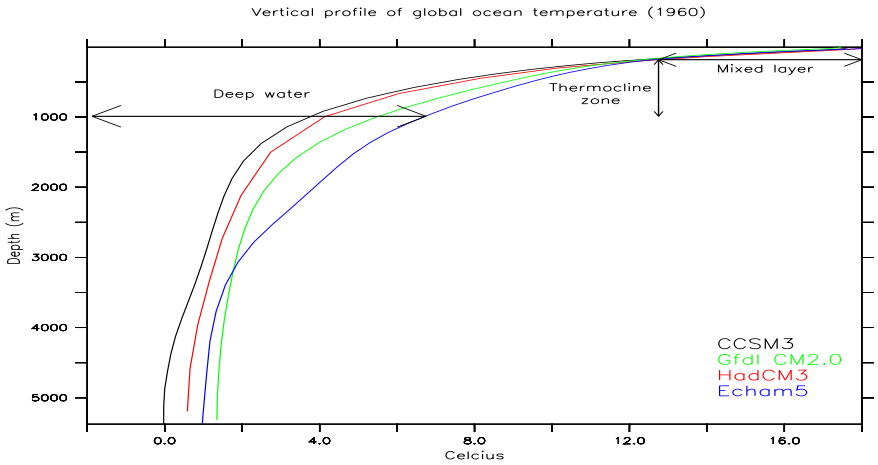

(b) Ocean

Figure 4.4: *Global averaged modeled vertical temperature profiles in the atmosphere (a) and ocean (b) for the year 1960.*

hPa there are some differences and also from 200 hPa to 10 hPa. Echam5 is 2-3 °C colder than the other models in the lower stratosphere. The temperature in Figure 4.4(a) is decreasing until approximately 100 hPa, and from thereon increasing. Thus the models do not reproduce the isotherm layer in the stratosphere from the tropopause to approximately 100 hPa. The temperatures are a bit warmer around 1000 hPa for the models than what is realistic: CCSM3 being the warmest while Echam5 being least warm. At the tropopause they are much colder than what is observed with Echam5 being the coldest. Echam5 is closest to the temperatures in

reality near the ground, but farthest away near the tropopause. Overall, the structure of the temperature profile for the models is realistic compared to Figure 3.1 in Liou (2002).

In reality the mixed layer in the ocean usually ranges from 50 to 200 m, and from 200 to 1000 m the temperature decreases rapidly which is called the thermocline (Pickard and Emery, 1982). The layer between the surface and approximately 1000 m is called the warm zone (Pickard and Emery, 1982). Below this is the cold zone, which is also called deep water and the temperature is approximately below 4 °C (Pickard and Emery (1982);Hartmann (1994, Figure 1.10)). In Figure 4.4(b) the vertical potential temperature profile for the ocean is shown. In the upper layer from 0 to 200 m, the temperature profiles are approximately the same for all the models. But from 200 m to the bottom, they are quite different. The coldest model is CCSM3, while the warmest is Echam5 down to approximately 3200 m and from there on Gfdl CM2.0 is the warmest one. CCSM3 is the most reasonable model, because the deep water is usually below approximately 4 °C and from around 1000 m. Echam5, on the other hand, does not reach 4 °C until 2000 m. The other three models have deep water between 1000 and 1500 m, which is more realistic. So the temperature profiles in the ocean for all the models are quite realistic in the upper 200 m while beneath that, CCSM3 and HadCM3 are best.

What is also evident is the close connection between ocean and atmosphere: at the surface the temperatures of ocean and atmosphere have almost the same value. This holds for all the models.

4.1.4 Results of comparing model simulations to observations

We will compare Figure 4.1 and 4.2 with Figure 4.3(a) qualitatively and look for differences or similarities on how the models fit with the observations of the ocean heat content and the surface air temperature. In the figures for ocean heat content, we can see that from 1950 to 1965 the V-models follow the observations better than the non-V models. This is the opposite of what is shown in Figure 4.3(a). Maybe the surface air temperature is not so closely connected with the ocean heat content in reality like what is simulated for the V-models where the peak in 1950 to 1965 is obvious in both Figure 4.1 and 4.3(a). The ocean heat content for the non-V models is a bit closer to the observations than for the V-models after 1970, while the surface air temperature for the V-models is closer to the observations than for the non-V models in that period. We find the V-models to be best mostly of the time, and maybe CCSM3 even better than Gfdl CM2.0. But overall, the models reproduce ocean heat content and global surface air temperature quite well. These results from comparing models with observations justify our study so that we can continue our work in studying the modeled ocean heat content and its impact on

the Earth's heat budget. Because of this, we can also assume that the energy fluxes, that we will study, are relatively realistic.

4.2 Qualitative description of modeled changes in the energy content during the 20th century

We will here study the vertical temperature changes with time in the ocean and in the atmosphere. The coupling between the ocean and the atmosphere will also be investigated, and a comparison of the models will be performed. In the ocean we choose to look at the temperature changes all the way down to 2000 m because it is important to see how these changes penetrate further down in the ocean even though it is the upper layer that reacts immediately to changes in the surface energy balance.

From the previous section, we found CCSM3 to be the best model. In Figure 4.5 (lower), the deep ocean for CCSM3 is cooling during the entire model run. For Gfdl CM2.0 in Figure 4.6 (lower), the deep ocean is warming. This warming is also slightly evident in the non-V models (Figure 4.7 and 4.8 (lower)). Gleckler et al. (2006) compared simulations of ocean heat content with observations from the World Ocean Atlas (WOA04) which is primarily qualitative. Most of the models examined in Gleckler et al. (2006) exhibited a significant drift over time in global ocean heat content, but for most of the models less than 10% of the drift occurred in the upper 250 m. The largest drift in many models is shown to be in the deep ocean. In fact, we will see in the next section that there is an unbalanced drift in all the models which is why we choose to disregard the deep ocean and focus on the upper 300 m of the ocean (section 4.3).

4.2.1 Coupling between air and sea

There is a very close connection between the contour plots of atmospheric temperature and ocean temperature shown in the following pages. Cooling and warming events which are evident in the atmosphere are also evident in the ocean, and they usually occur in the same periods. The only difference is that in the atmosphere a cooling or warming penetrates quickly through the entire troposphere and is often short-lived (a few years), while in the ocean a penetration is usually slow and long-lived, depending on the model. Even though we find the models to have a close connection, there are some occurrences of cooling or warming in the lower troposphere which are not evident in the upper ocean, or vice versa. We also saw this for the observations in section 4.1 which we will discuss further at the end of this section.

4.2.2 Temperature development in the troposphere and the stratosphere

The troposphere and the stratosphere have opposite trends during the 20th century: there is a gradual cooling above 100 hPa in the stratosphere while a warming in the troposphere (below 200-300 hPa). The isotherm layer is between the tropopause and 100 hPa which we mentioned in section 4.1. This is slightly evident in all the models (green color around 100 hPa which has an anomaly of approximately zero, i.e. no change), but in Figure 4.4(a) this was not obvious. In Figure 4.4(a) (section 4.1) the vertical temperature profile had a shift in the temperature trend at approximately 100 hPa: it was decreasing from 1000-100 hPa, while increasing from 100-10 hPa. As we can see from the figures here, the isotherm layer is very small so this is probably why it is not evident in Figure 4.4(a).

The lower troposphere is warming during the 20th century due to the increase in greenhouse gases from approximately 1950 (see section 2.2) which absorb radiation. This is why the stratosphere is cooling, not only due to the absorption in the troposphere, but also due to a significant increase in CO_2 concentration (Le Treut et al., 2007, IPCC) which results in more emissions of thermal radiation (Hartmann, 1994, Figure 3.18), and also a decrease in total ozone concentration (Fioletov et al., 2002, Figure 3) which results in a smaller absorption of SW radiation. This again will also contribute to additional warming of the lower troposphere because more SW radiation reaches the ground along with emissions of LW radiation. When there is a major volcanic eruption, on the other hand, a large amount of aerosols will reach the stratosphere, hence there will be a warming in the stratosphere and a cooling in the troposphere. This is mainly due to the reflection of SW radiation by the aerosols so that less SW radiation reaches the ground and so that more is absorbed in the stratosphere.

4.2.3 The difference between models with or without volcanic forcing

V-models

CCSM3 and Gfdl CM2.0 are, as we mentioned earlier, the models with variations in natural and anthropogenic forcing. Because of this we will study how volcanic and solar forcing influence the temperatures in the atmosphere and in the ocean. During the late 19th century and the 20th century there were five major volcanic eruptions which will be focused on here, namely that of Krakatoa (Indonesian) in 1883, of Santa Maria (Guatemala) in 1902, of Agung (Bali) in 1963, of El Chichon (Mexico) in 1982 and of Pinatubo (the Philippines) in 1991 (from Figure 8.13 in Liou (2002)). The most powerful eruption was Krakatoa in 1883, and the

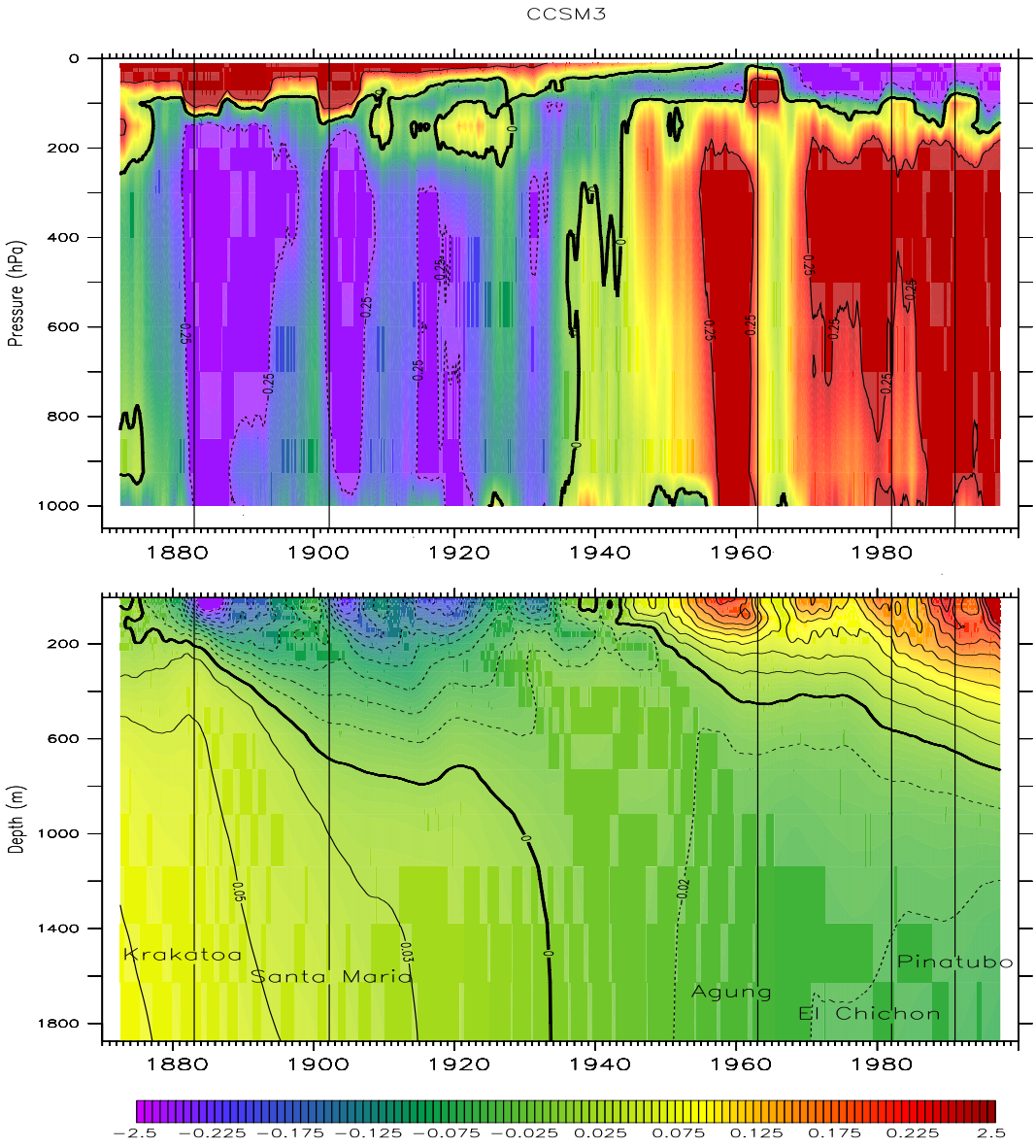

Figure 4.5: *(Upper) Air temperature anomalies (1000-10 hPa) in CCSM3, and (Lower) Potential sea temperature anomalies (0-2000 m) in CCSM3. The anomalies are relative to 1870-1999.*

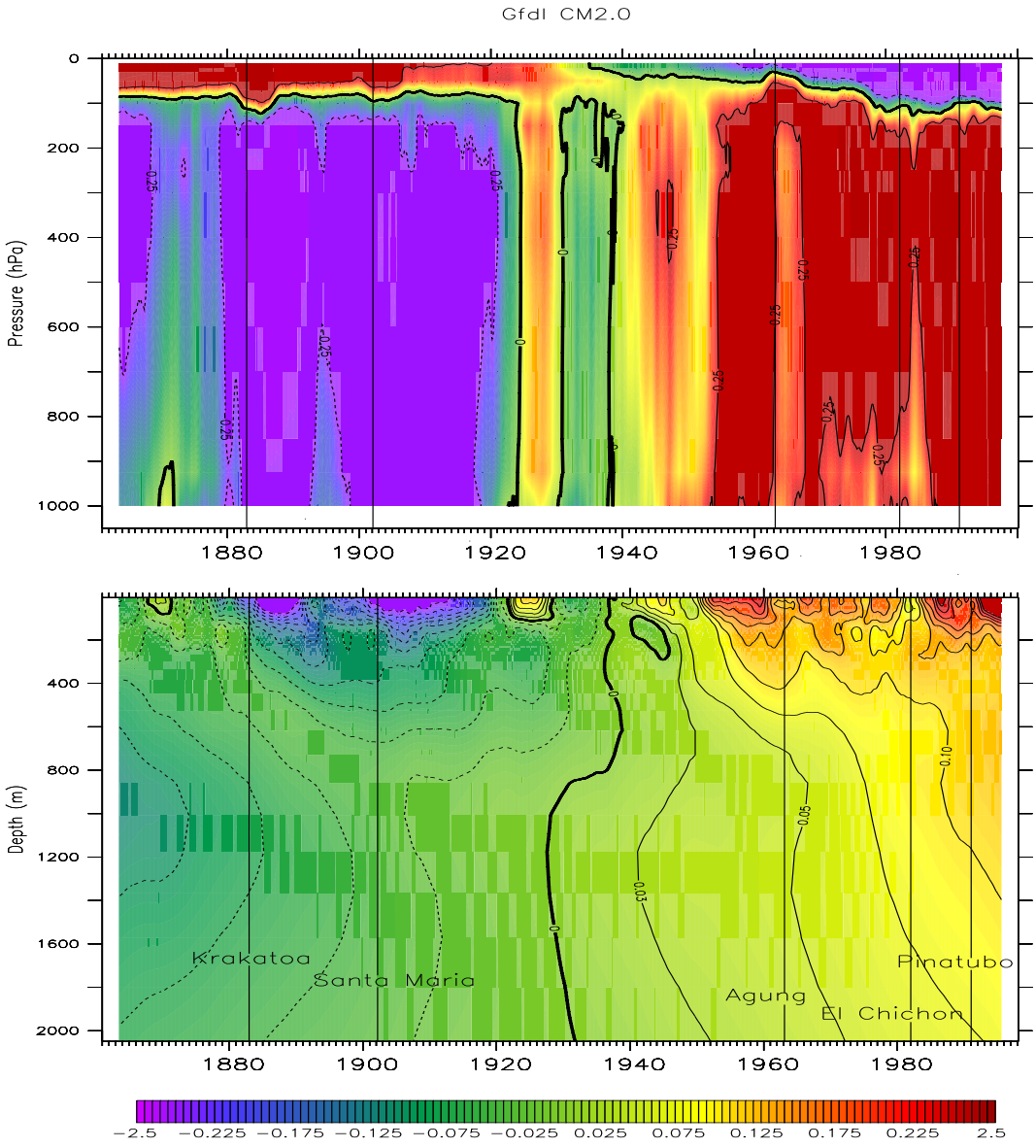

Figure 4.6: *(Upper) Air temperature anomalies (1000-10 hPa) in Gfdl CM2.0, and (Lower) Potential sea temperature anomalies (0-2000 m) in Gfdl CM2.0. The anomalies are relative to 1861-2000.*

next most powerful was Pinatubo in 1991. The incoming solar radiation started to increase in the early 1900s until approximately 1960 (Hartmann, 1994, Figure 11.3).

After Krakatoa (1883) and Santa Maria (1902) there is a strong cooling in the surface layer of the ocean (down to 200-300 m) for CCSM3 and Gfdl CM2.0 (see Figure 4.5 and 4.6 (lower), respectively), and also in the atmosphere (see Figure 4.5 and 4.6 (upper)). The cooling is evident throughout the entire troposphere and in the lower stratosphere (up to approximately 100 hPa) and continues to the early 1930s which applies to both CCSM3 and Gfdl CM2.0. There is one exception for Gfdl CM2.0 and that is a heating in the late 1920s evident in the atmosphere and slightly in the ocean. At the ocean surface, the cooling after Krakatoa and Santa Maria immediately reaches down to approximately 200 m depth for both the models, but a difference in how the cooling penetrates further down in the deep ocean is evident: in CCSM3 the cooling penetrates slowly (goes over decades), while in Gfdl CM2.0 the penetration is quick and immediately located down to 2000 m.

In the early 1940s for CCSM3 and the late 1930s for Gfdl CM2.0 a significant increase in the temperature in the surface ocean layer and throughout the troposphere is evident which is a combination of significantly increased greenhouse gas concentration from approximately 1950 (Le Treut et al., 2007; Forster et al., 2007, IPCC) and the increase in incoming solar radiation from the early 1900s until approximately 1960. There are three major volcanic eruptions after 1960 as well as a large amount of anthropogenic aerosols (mentioned in section 2.2), but still the upper ocean continues to heat up, which is also evident in the atmosphere (Figure 4.5 and 4.6 (upper)). This must come from the fact that the concentration of greenhouse gases in the atmosphere started to increase significantly from approximately 1950 and that there was a decrease in anthropogenic aerosols from the 1980s. When the ocean is heated, it will get a stronger stratification. Thus a cooling due to volcanic and anthropogenic aerosols is less powerful in cooling the ocean. The warming penetrates further down in the ocean, like we saw for the cooling events, but the same difference between the models is still evident: penetration is quicker in Gfdl CM2.0 than in CCSM3. In reality a vertical penetration of heat in the ocean is not as quick as in the atmosphere. CCSM3 is therefore more realistic. But in the upper 300 m of the ocean, we can see a similar development for both the models: there is a clear warming during the 20th century. Also on this basis, as well as the drift in the deep ocean, we will concentrate on the upper 300 m of the ocean.

Non-V models

The temperature distribution for HadCM3 and Echam5 (non-V models) in Figure 4.7 and 4.8 is quite different from that in the V-models, even though the connection between ocean and atmosphere is quite good. In the upper ocean the significant warming event starts in the early 1970s for HadCM3 and Echam5. This is 20-30 years after the warming starts in the V-models (the 1940s). There is no significant cooling in the surface layer of the ocean, only small, but quite strong events (blue-purple dots in the upper 50 m shown in Figure 4.7 and 4.8 (lower)) which occur differently for the models. In the deep ocean, the temperature is slightly increasing, but the change is not as significant as for the V-models. And compared to the atmosphere, the deviations are much stronger.

In the atmosphere there are more cooling events before the early 1970s than in the upper ocean. There are also some small warming events in between which is also evident in the surface layer of the ocean, but these events do not occur until the late 1910s for HadCM3 and the early 1930s for Echam5. In HadCM3 there is a clear warming event in the atmosphere in the late 1910s that lasts for a few years. This warming event is also evident in the ocean, but occurs a few years earlier at 200-300 m depth. The warming event in the atmosphere could then be due to a release of heat from the ocean, i.e. an internal oscillation in the ocean. In Echam5 there is also a clear warming event in the atmosphere in the early 1930s. In the ocean the warming is located at 100 m a few years earlier and approximately 20 years earlier at 900 m. In the non-V models there are therefore occurrences where the ocean might be responsible for warming in the atmosphere which implies internal oscillations in the ocean. In the V-models this is not obvious which might be due to a dominating variation in volcanic and solar forcing. This will be studied further in section 4.4.

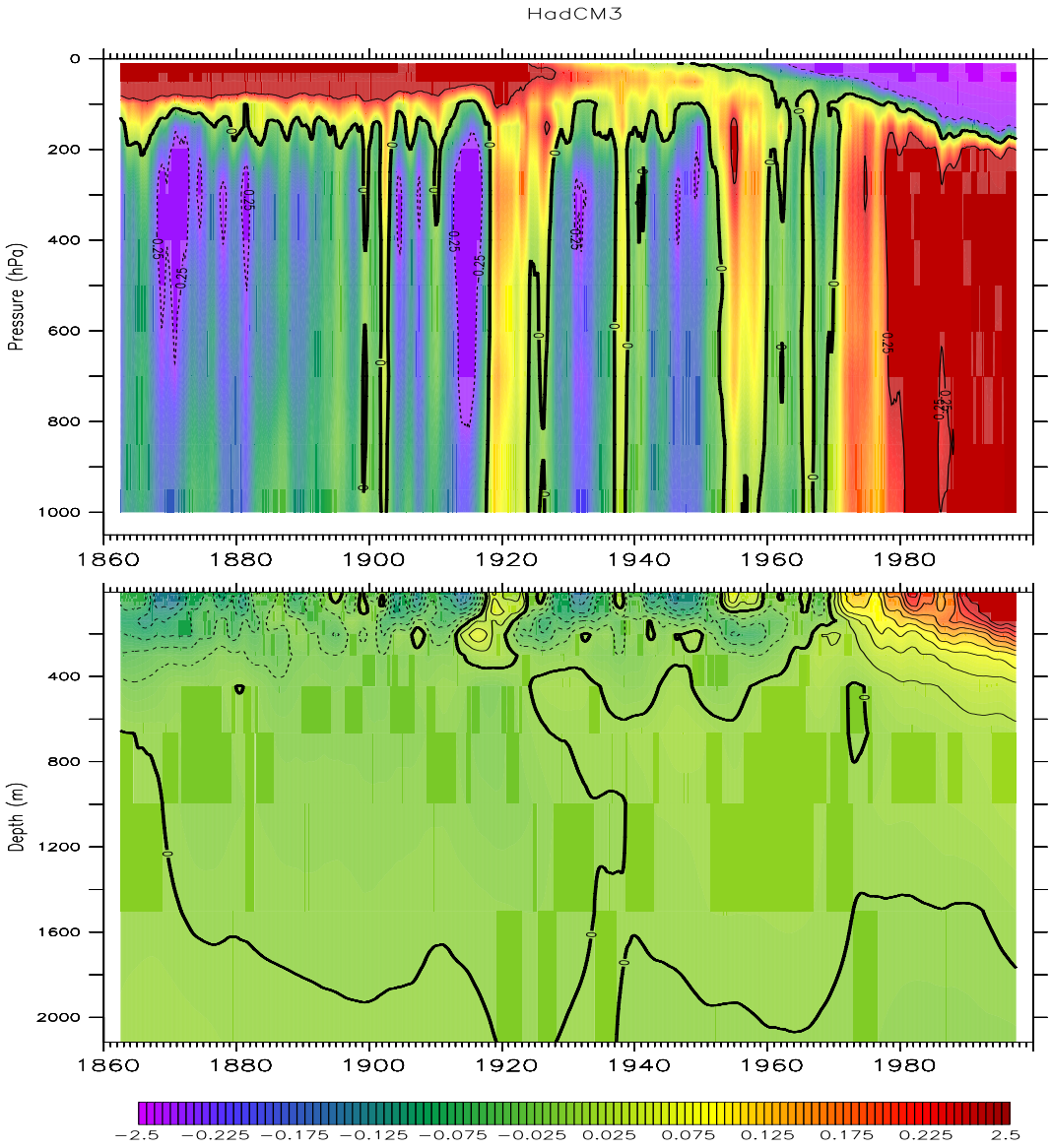

Figure 4.7: *(Upper) Air temperature anomalies (1000-10 hPa) in HadCM3, and (Lower) Potential sea temperature anomalies (0-2000 m) in HadCM3. The anomalies are relative to 1860-1999.*

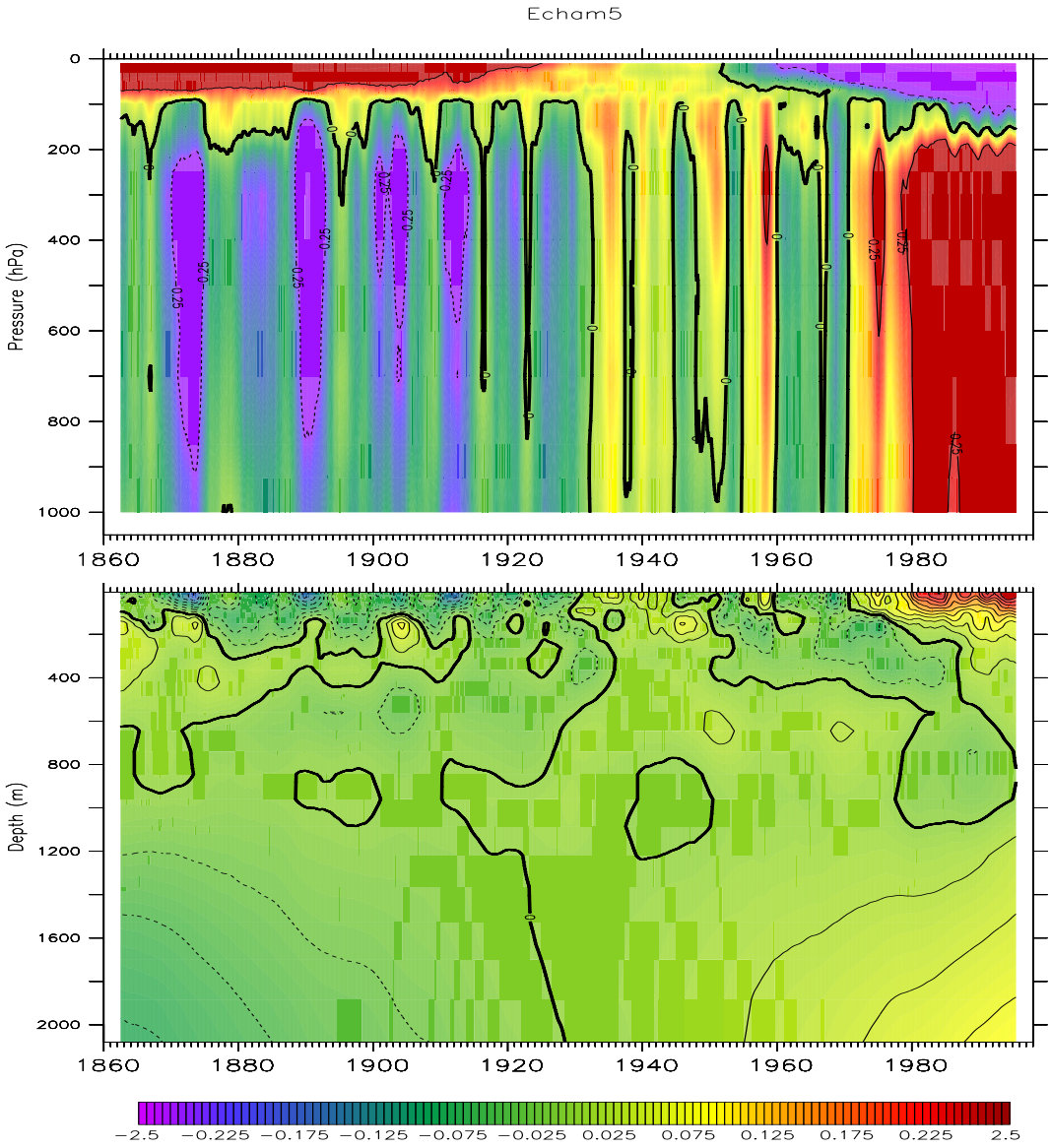

Figure 4.8: *(Upper) Air temperature anomalies (1000-10 hPa) in Echam5, and (Lower) Potential sea temperature anomalies (0-2000 m) in Echam5. The anomalies are relative to 1860-1999.*

4.2.4 How realistic are the models?

Temperature changes in the atmosphere and in the ocean do not always follow each other which we also saw for the observations in section 4.1 (see Figure 4.1, 4.2 and 4.3(a)). We will then from the previous section (4.1) use the result of comparing modeled simulations and observations of ocean heat content (0-300 m) and global surface air temperature to compare with the vertical contour plots of the atmosphere and the ocean. We choose three periods which we find important to compare with: after a volcanic eruption (1900-1910), the significant peak obvious in OHC-observations (1950-1965) and in 1980-1999 which was after the greenhouse gases already had started to increase significantly (from approximately 1950) which was not evident in the OHC for the V-models until 1980.

After the Santa Maria eruption in 1902, the global surface air temperature observations (both NASA and HadCRU) is decreasing which is also clearly evident for the V-models (CCSM3 and Gfdl CM2.0). HadCM3 and Echam5 do not have volcanic forcing so that there is not a significant decrease during this period of time like for the V-models. The V-models have the best fit to the observations in this period: CCSM3 is close to the observations from NASA (2009), while Gfdl CM2.0 is close to HadCRUT3 (observations from Jones and Salmon (2008)). This is just due to where the zero-crossing is set which is different for the two observation datasets. In the upper of Figure 4.5 and 4.6 there is clearly a continuous cooling for the V-models, which is also slightly evident for the non-V models as well, in Figure 4.7 and 4.8 (upper). For the period of 1900 to 1910, the V-models are more realistic than the non-V models which is because of the volcanic forcing.

We found the V-models to be best in 1950 to 1965 for the ocean heat content (0-300 m), while the non-V models (HadCM3 and Echam5) performed best for the global surface temperature in the same period (section 4.1). If we compare the lower of Figure 4.5 and 4.6 with the period of 1950 to 1965 for the ocean heat content in section 4.1 (Figure 4.1), where OHC increased from 1950 to 1960 and decreased to around 1965, we can see that the increase and decrease is also evident in the ocean layer from 0 to approximately 200 m. For the non-V models, on the other hand, this is not obvious: the increase in the upper ocean does not start until approximately 1970 in the contour plot of the ocean which is also evident in section 4.1 (Figure 4.2). For the global surface air temperature in section 4.1 (Figure 4.3(a)), a heating is obvious from 1950 to approximately 1960 for all the models which is also evident in the contour plot of the atmosphere. But the non-V models are anyhow closer to the observations. For the period of 1950 to 1965, the V-models are most realistic for the upper ocean while the non-V models are most realistic for the global surface air temperature.

After the significant increase in greenhouse gases in the middle of the 20th

century, the ocean heat content and the global surface temperature started to increase, as seen in section 4.1. In the period of 1980 to 1999, there is a clear increase in both OHC and global surface air temperature which is evident in all the models. This significant increase is also evident in the contour plots of the atmosphere and the ocean (Figure 4.5, 4.6, 4.7 and 4.8). The non-V models reproduce the ocean heat content better during this period than the V-models whereas the V-models reproduce the global surface air temperature better. Even though the non-V models reproduce the ocean heat content better, the decadal variability like in the V-models, are not there.

Overall, the models are not precise, but they reproduce ocean heat content in 0-300 m and global surface air temperature quite well, especially after 1970.

4.3 Quantitative analysis of Earth's energy budget during the 20th century

We will now investigate the ocean heat content (OHC) during the 20th century more in detail and study how changes in the energy budget of the Earth affect the OHC and also the atmospheric heat content (AHC). To do this, we first start by investigating the drift in the ocean we saw in the previous section, and then we will compare OHC with the net energy balance to see how they connect. Next we will study the development in OHC and AHC, and finally look at three case studies: Case 1) Cooling after a volcanic eruption, Case 2) Recovery after a volcanic eruption, and Case 3) Warming due to greenhouse gases.

4.3.1 Drift in deep ocean

Remember, we saw a drift in the deep ocean in all the models in the previous section. We will here investigate what causes this drift. First we will use two different methods to compute the total change in OHC during the 20th century. The first method is to use Ferret (section 3.3) which integrates the potential temperature (Θ) with depth and area, and then compute the difference in OHC by subtracting the first year from the last to get the total change during the 20th century. The second method is to calculate the OHC from the surface net energy flux (F_{net} from equation (2.5)). We will now check if these two methods of computing the total change in OHC give the same results. In the second method we will use equation 3.9 from Knauss (1997) to compute the ocean heat content:

$$\int_0^t Q_T \, dt \; = \; \int_0^Z c_p \rho \Delta T \, dz, \tag{4.1}$$

where Q_T is the same as F_{net}. An integration of Q_T over time gives the heat in a surface layer Z, but what we want is the total global ocean heat content. To achieve this we have to integrate F_{net} over area (dxdy), as well as in time (dt), since the unit for OHC and F_{net} is Joule and W/m^2, respectively. The equation for OHC is then:

$$OHC = F_{net}\, dt\, dxdy\,, \tag{4.2}$$

where dxdy is the same as equation 3.4 and is approximately 70% of the total surface area of the Earth, i.e. the surface area of the ocean which is given in Table 4.1 for all the models (computed in Ferret). From the equation above, the OHC results in the heat content for the total depth of the ocean. This is shown in Table 4.2. In the table are also the values for OHC computed from the integration of Θ for the total depth and for 0-300 m.

Model	**Ocean surface area**
CCSM3	$3.632 \cdot 10^{14}$
Gfdl CM2.0	$3.324 \cdot 10^{14}$
HadCM3	$3.623 \cdot 10^{14}$
Echam5	$3.629 \cdot 10^{14}$

Table 4.1: *Global ocean surface area for all the models which we use in the computation of ocean heat content (method 1). These surface areas are computed in Ferret.*

From Table 4.2 a computation of OHC from the net energy flux results in much greater values than the OHC computed from the potential temperature for all the models. This means that there is an imbalance in the model's energy budget, i.e.

Model	**1)** OHC_{Q_T}	**2)** OHC_Θ **(total)**	**2)** OHC_Θ **(0-300 m)**
CCSM3	$-8.086 \cdot 10^{23}$	$-6.04 \cdot 10^{23}$	$1.21 \cdot 10^{23}$
Gfdl CM2.0	$2.843 \cdot 10^{24}$	$9.06 \cdot 10^{23}$	$1.30 \cdot 10^{23}$
HadCM3	$1.082 \cdot 10^{24}$	$5.83 \cdot 10^{22}$	$1.53 \cdot 10^{23}$
Echam5	$1.368 \cdot 10^{24}$	$6.20 \cdot 10^{23}$	$3.97 \cdot 10^{22}$

Table 4.2: *Ocean heat content computed in two different ways: 1) from the net energy balance, and 2) from the potential temperature which is the difference between OHC in the last and the first year (CCSM3: 1999-1870, Gfdl CM2.0: 2000-1861, HadCM3 and Echam5: 1999-1860).*

the energy is supplied or extracted from the ocean which can not be accounted

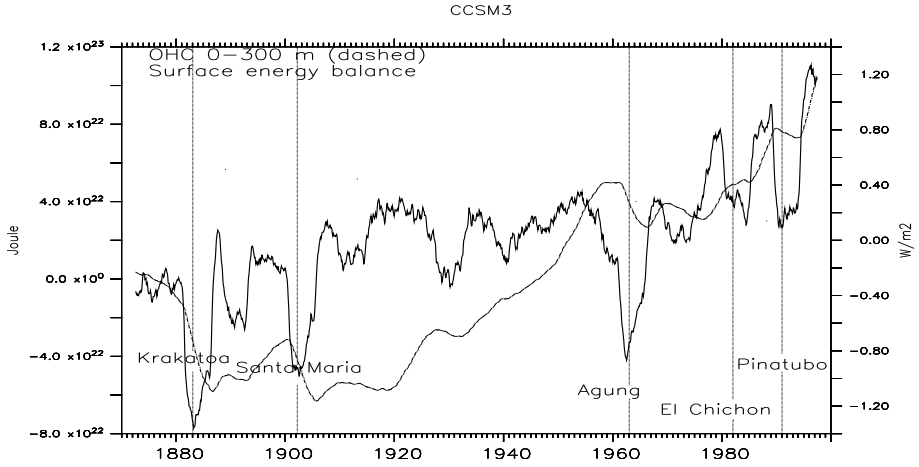

(a) CCSM3

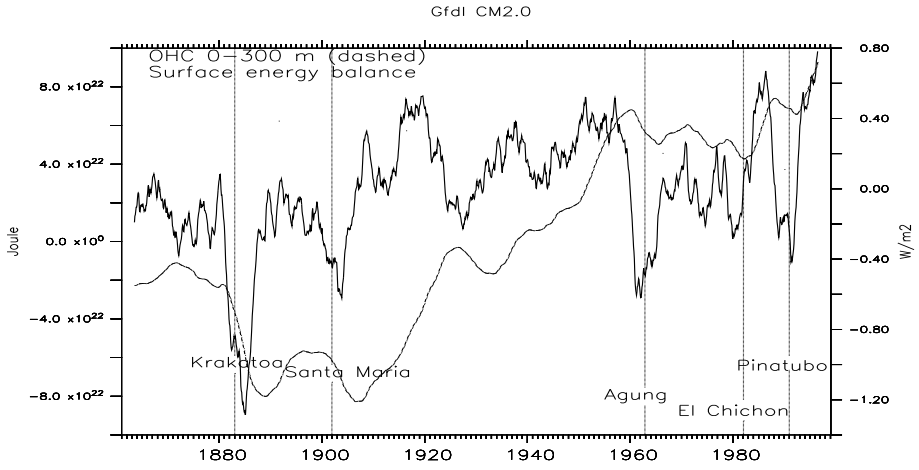

(b) Gfdl CM2.0

Figure 4.9: *Ocean heat content (0-300 m) and surface net energy balance anomalies over ocean for CCSM3 and Gfdl CM2.0. The time series are relative to 1870-1999 for CCSM3 and 1861-2000 for Gfdl CM2.0. The OHC (dashed) is pursuant to the left y-axis, while the surface energy balance (solid) is pursuant to the right.*

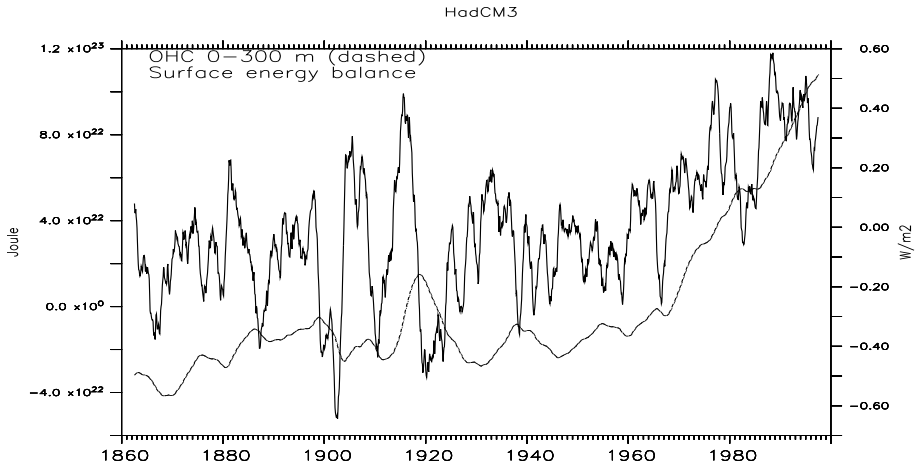

(a) HadCM3

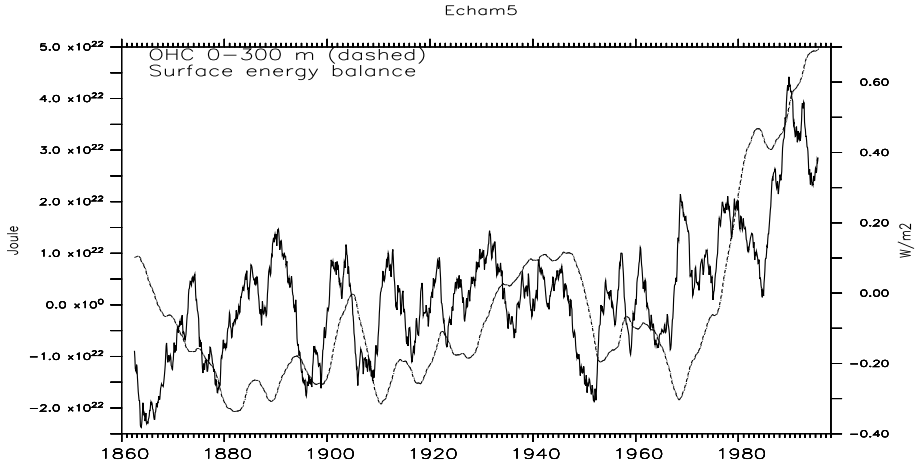

(b) Echam5

Figure 4.10: *Ocean heat content (0-300 m) and surface net energy balance anomalies over ocean for HadCM3 and Echam5. The time series are relative to 1860-1999. The OHC (dashed) is pursuant to the left y-axis, while the surface energy balance (solid) is pursuant to the right.*

for by the air-sea energy fluxes. Therefore we can not perform an exact energy budget for the models. Nevertheless, we can see in Figure 4.9 and 4.10 that there is a relationship between the net energy flux and the OHC for 0-300 m: when less energy is transferred through the sea surface, the ocean becomes colder (example in Figure 4.9(a) around 1900, 1930, 1960 etc.). And from what we experienced in the comparison of model simulations with observations, we could see that the ocean heat content in 0-300 m fits quite well with the observations. Because of this qualitative relationship we still feel satisfied to continue our study.

4.3.2 Ocean heat content

Now we will study the development in OHC in more detail and compare the all models (in section 4.1 earlier, we compared modeled ocean heat content to observations, but in that case we were limited by the observations which only cover the period 1950-1999). In Figure 4.11 the anomalies for OHC (0-300 m) during the 20th century are shown for all the models. Since CCSM3 is only given for 1870-1999, we plot the other models for this period as well. The volcanic eruptions mentioned in the previous section are evident here for the V-models: when there is a volcanic eruption, OHC decreases. The largest decrease in OHC for CCSM3 and Gfdl CM2.0 is after the Krakatoa eruption in 1883 which was the most powerful eruption during the late 19th and the 20th century. After the Krakatoa and Santa Maria eruptions, OHC starts to increase significantly for CCSM3 and Gfdl CM2.0 until the early 1960s. This large increase is not only due to the recovery after the volcanic eruptions, but also due to the increase in incoming solar radiation that was evident from the early 1900s to approximately 1960 (Hartmann, 1994, Figure 11.3). In the early 1960s there is a decrease in OHC for the V-models which is due to major volcanic eruptions (Agung in 1963 and El Chichon in 1982) and also due to the significant increase in anthropogenic aerosols which reached their maximum in the 1980s (Stern, 2005). In the non-V models, however, there is no significant increase in the OHC until around 1970. This latter development is a result of only variability in the anthropogenic forcing.

The first two eruptions (Krakatoa and Santa Maria) and the Agung eruption provoke a cooling in the V-models that starts at the same time in CCSM3 as in Gfdl CM2.0. The non-V models are very different from the V-models from the beginning to the late 1920s. A large decrease in OHC is evident in CCSM3 and Gfdl CM2.0 from approximately 1880 due to the major volcanic eruptions in 1883 and 1902. From 1906, the OHC in the V-models starts to increase, not only as a response to a recovery after the eruptions, but also as a response to the increase in incoming solar radiation. There was also a very small volcanic activity during this period of time (Liou, 2002, Figure 8.13). The non-V models, on the other hand, have no significant trend from 1870 to approximately 1970. In the period from

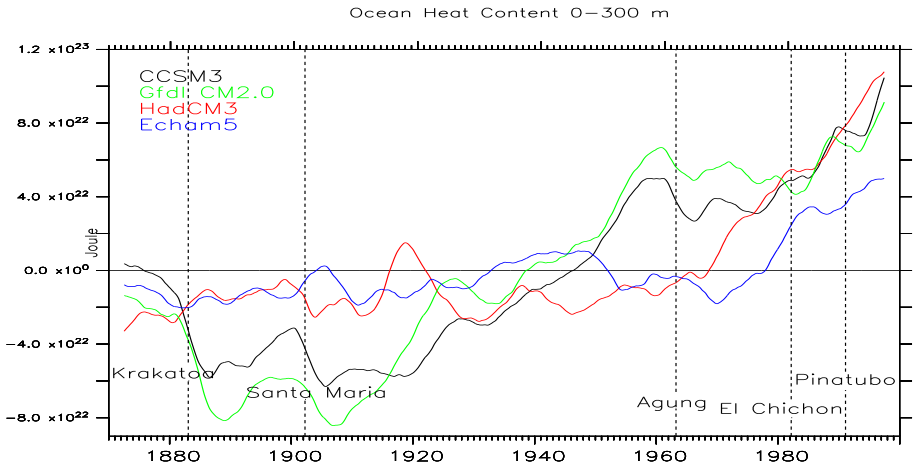

Figure 4.11: *Ocean heat content anomalies in 0-300 m for all the models. The anomalies are relative to 1870-1999.*

the late 1920s until year 1950, all the models are much closer to each other than before. After this, the V-models have a great peak until 1965 which is not evident in the non-V models. We also found this in the comparison of modeled and observed OHC in section 4.1 where the V-models were closest to the observations in that period (1950-1965). The increase is slightly evident for Echam5 in Figure 4.2 from section 4.1 as well, while in Figure 4.11 the increase is not evident. This can be explained by that we use different climatologies: in section 4.1 the anomalies are relative to 1950-1999, while here they are relative to 1870-1999. In the late 1970s and throughout the rest of the 20th century, all the models are close to each other and they almost reach the same value in 1999, except for Echam5 which lies much lower. This period was the period where the non-V models reproduced the OHC best (section 4.1) compared to the V-models, but remember that they did not reproduce the decadal variations in the observations like the V-models did.

We will further investigate how cooling and warming occur in the ocean by studying the energy fluxes. Since the V-models fit the observations best in the period 1950-1965 when the ocean was cooled due to a volcanic eruption, we will study how the energy fluxes act during cooling caused by volcanic eruptions in Case 1). There was also an increase in anthropogenic aerosols until the 1980s when maximum values were reached. Despite this, we still choose to study the cooling after volcanic eruptions. The periods we will study in Case 1) are year 1881-1887, 1901-1906 and 1961-1966 for CCSM3 and year 1881-1889, 1897-1907 and 1960-1965 for Gfdl CM2.0. Then it is also important to investigate a recovery after a volcanic eruption which we will do in Case 2): periods 1887-1901,1906-1926 and 1966-1981 for CCSM3, and 1889-1897, 1907-1925 and

1965-1986 for Gfdl CM2.0. The significant increase due to greenhouse gases after 1960 in the non-V models is also important to investigate which is also evident in the V-models even though there are three major volcanic eruptions and anthropogenic aerosols present. But as we can see in Figure 4.11, the increase in OHC for the V-models is mostly delayed due to the volcanic eruptions in 1963 and 1982 (Agung and El Chichon) and continues to increase after this, especially in CCSM3. In Case 3) we will therefore study the warming due to greenhouse gases where we will look at the period of 1980-1999 for CCSM3 and Gfdl CM2.0 from where the increase is clear in both the models and where there is no evidence of significant cooling anymore. In HadCM3 and Echam5, the period from 1969 to 1999 will be studied.

Notice the decrease in OHC for Gfdl CM2.0 in the 1920s which is also evident in CCSM3, but much smaller. There were no major eruptions during that period of time (Fig. 8.13 in Liou, 2002), so this may be an internal oscillation in the ocean. After 1960 as we mentioned above, the increase in OHC is weakened for the V-models. The significant increase in OHC continues in the late 1970s due to the great increase in GHGs that started in the middle of the 20th century and which eventually dominated the cooling effect by the volcanic and anthropogenic aerosols. If we look at the OHC for HadCM3 (red curve in Figure 4.11), we can also see a significant peak as for Gfdl CM2.0 that is occurring a bit earlier (1915-1930), even though the former is a model without volcanic forcing and variations in incoming solar radiation. This indicates the presence of internal oscillations in the ocean. We will investigate this later on in section 4.4, i.e. if the ocean sometimes is responsible for a cooling or a warming of the climate system.

4.3.3 Atmospheric heat content

Since we study the OHC, we will also study AHC to see how the OHC relates to the AHC and to find differences between the troposphere and the stratosphere. In Figure 4.12(a) a positive trend is evident in the troposphere during the 20th century while in the stratosphere (Figure 4.12(b)) there is a negative trend for all the models. This was also obvious in the contour plots for the amtosphere in the previous section (Figure 4.5, 4.6, 4.7 and 4.8). In reality when there is a warming in the lower troposphere there is a cooling in the stratosphere due to changes in the composition which we discussed in section 4.2.2 (also in section 2.2). It is also obvious that the troposphere holds most of the heat content of the atmosphere: tropospheric heat content anomalies are a factor 10 larger than the stratospheric heat content anomalies, i.e. changes in the troposphere result in much larger changes in the heat content than in the stratosphere. This is because the troposphere has a larger amount of mass due to the pressure level range from 1000 hPa to 200 hPa approximately, while the stratospheric heat content we calculate here is only from

200 hPa to 10 hPa.

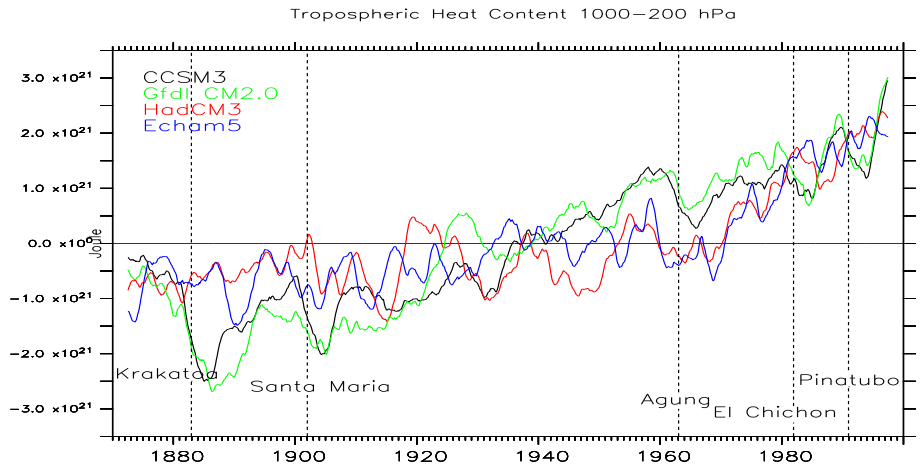

(a) THC

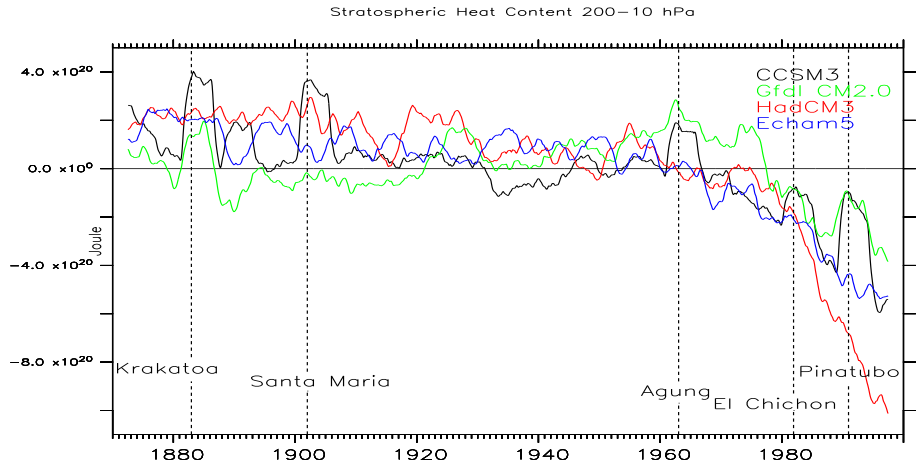

(b) SHC

Figure 4.12: *a) Tropospheric heat content anomalies in 1000-200 hPa layer, and b) Stratospheric heat content anomalies in 200-10 hPa layer. Anomalies are relative to 1870-1999.*

Figure 4.12(a) shows the heat content computed for 1000-200 hPa in the atmosphere which is defined as the troposphere. If we look closer, we can see that the variations in the anomalies for the tropospheric heat content (THC) are not so different between the models compared to how different they are for the OHC. What is clearly similar between the models is that the V-models start to increase around 1920 for both OHC and THC, as a response to the recovery after the major volcanic eruptions in 1883 and 1902, while the non-V models do not start to

increase significantly until the late 1960s. In Figure 4.12(b) the stratospheric heat content (SHC) for each model is shown where we can see a clear decrease during the 20th century which was also evident in the contour plots in section 4.2. The volcanic eruptions are visible in the SHC for CCSM3, but for Gfdl CM2.0 they are not that visible. So maybe the connection between the troposphere and the stratosphere is not so well related to each other in Gfdl CM2.0 as in CCSM3.

In Delworth et al. (2005) the time series of the ocean heat content in 0-3000 m has the apperance of a low-pass filtered signal. This is because the ocean acts as a time-integration of net energy imbalances. The surface air temperature on the other hand responds more quickly to changes in radiative forcing (Delworth et al., 2005). This is also evident in the models we study, even though we only look at the ocean heat content in 0-300 m: THC, as well as SHC, has a lot of small variations in periods where the variations are not visible in the ocean heat content (0-300 m) because the ocean responds to greater changes which is due to inertia in the ocean. Next, we will see this even clearer when we study the energy fluxes and the OHC.

4.3.4 Case 1) Cooling after a volcanic eruption

After a major volcanic eruption, there will be aerosols reaching the stratosphere (where they have long lifetime) causing a cooling of the climate system. We will therefore study the energy fluxes, especially the surface fluxes over ocean, when there is a cooling in the ocean due to a volcanic eruption. In this way we can see which fluxes that contribute most to a cooling. In Figure 4.13 and 4.14 the OHC and the energy fluxes for the V-models (CCSM3 and Gfdl CM2.0) are shown where the cooling events are marked by C1 (as in Case 1). The fluxes are separated into two figures for each model to see how even fluxes with small variability occur: SW_{down}, SW_{refl}, SW_{out} (TOA), LW_{down}, LW_{up} and LE in the upper figure, and SW_{in} (TOA), SW_{up}, SW_{abs}, LW_{out} (TOA) and SH in the lower figure.

SW_{in} at TOA oscillates in its own way due to the well known 11-year sunspots cycle, so temperature changes in the climate system are not due to the oscillations in incoming solar radiation, but mostly due to changes in the composition of the atmosphere, especially aerosols from volcanic eruptions which cause abrupt changes.

By studying Figure 4.13 and 4.14 for C1 events, it is obvious that SW_{down} is occurring first. After this, LW_{up} is occurring approximately at the same time as LW_{down} which seems to be the case for the other fluxes as well. During a volcanic eruption, the accumulation of aerosols in the atmosphere, especially in the stratosphere, results in a direct effect through a reflection of SW radiation. This reflection also results in less absorption of SW radiation in the troposphere

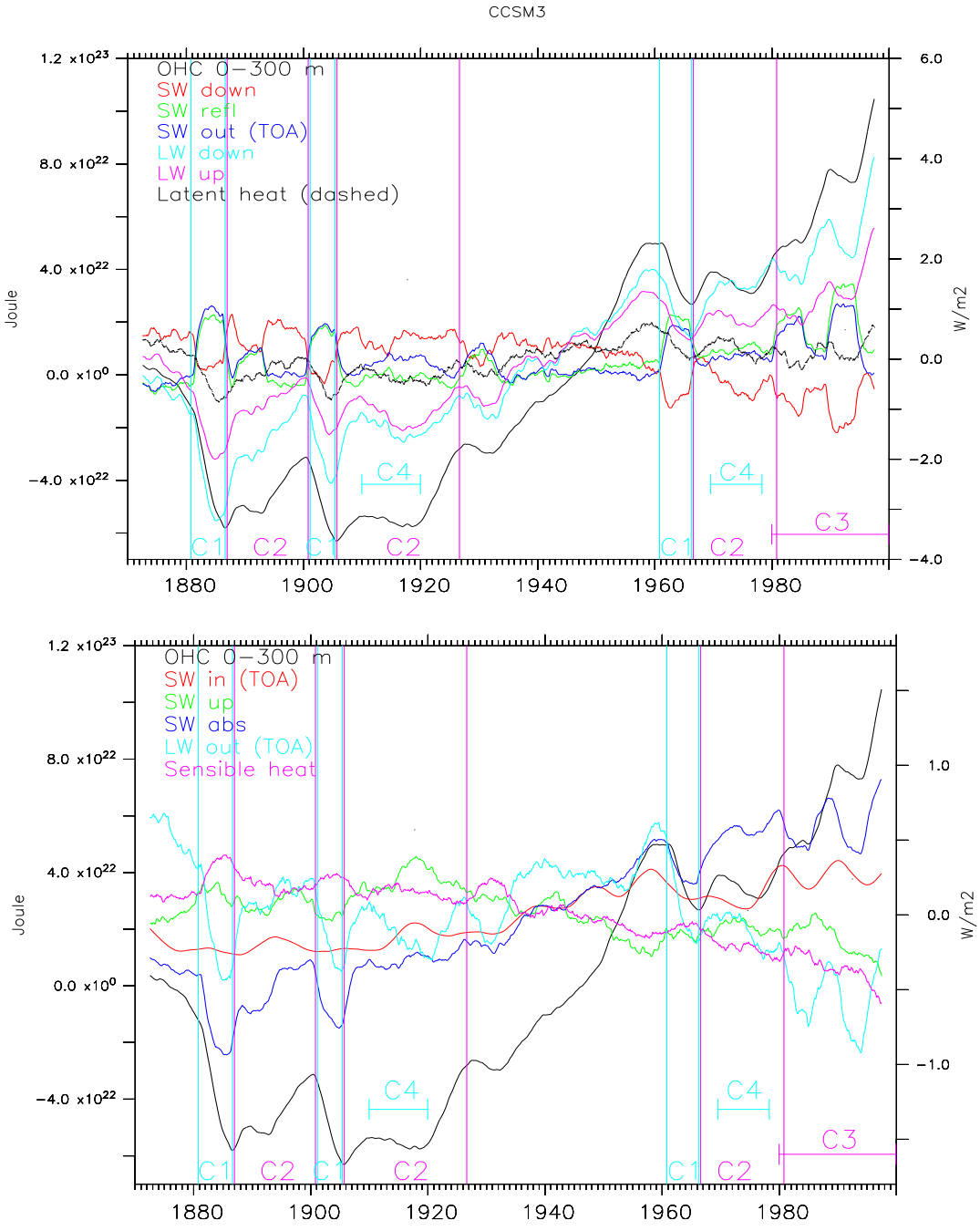

Figure 4.13: *Ocean heat content (0-300 m) and different energy fluxes in CCSM3 where the surface fluxes are over ocean only and the rest are global. (Upper) Flux components with the largest anomalies and (Lower) Flux components with the smallest anomalies. The anomalies are relative to 1870-1999. (Left y-axis: OHC; right y-axis: energy fluxes)*

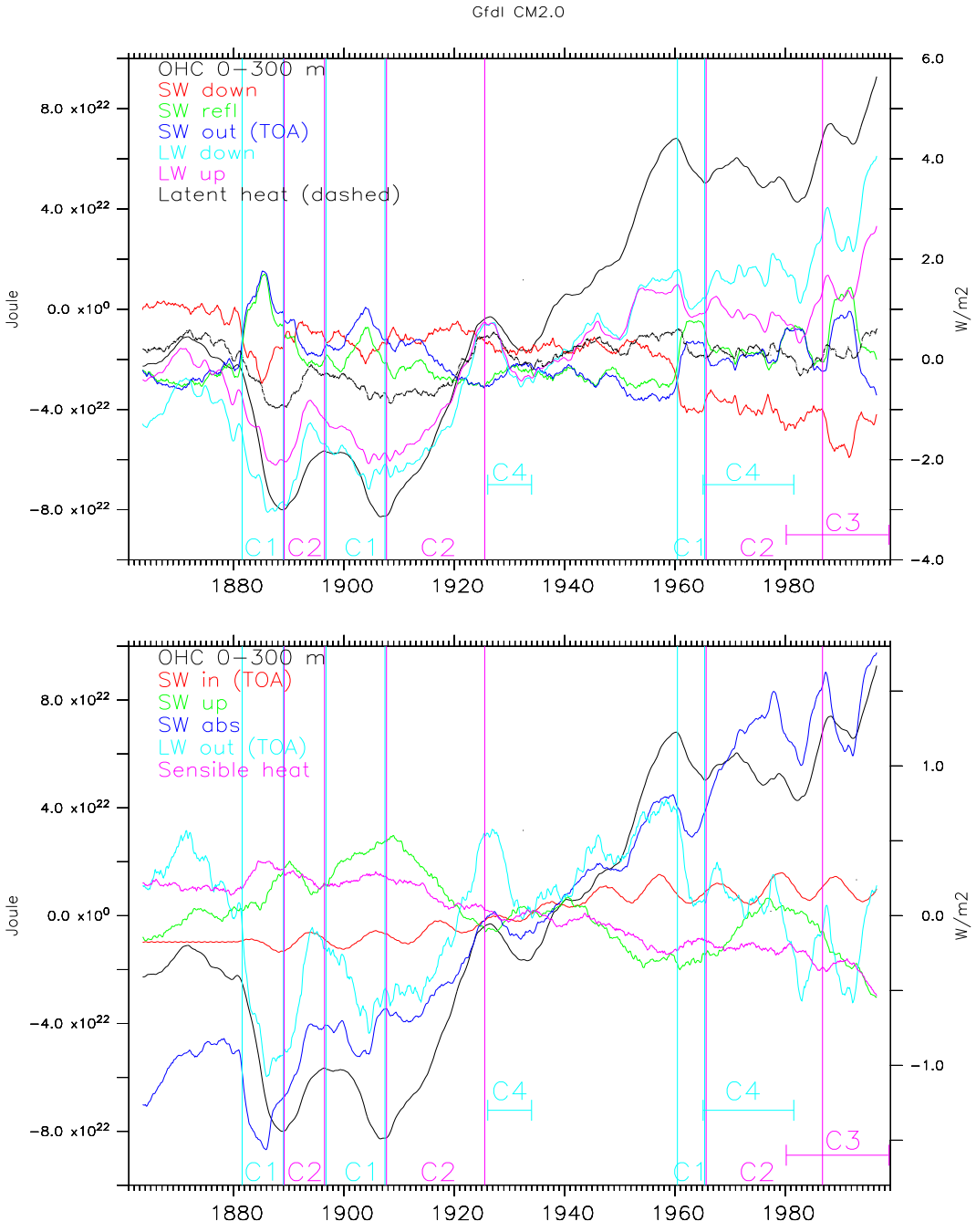

Figure 4.14: *Ocean heat content (0-300 m) and different energy fluxes in Gfdl CM2.0 where the surface fluxes are over ocean only and the rest are global. (Upper) Flux components with the largest anomalies and (Lower) Flux components with the smallest anomalies. The anomalies are relative to 1861-2000. (Left y-axis: OHC; right y-axis: energy fluxes)*

and less SW radiation reaching the ocean. And since the ocean then cools, there will be less LW radiation emitted from the ocean and also a reduction in LE. Because of these factors there will be less downwelling LW radiation emitted down to the surface which again results in cooling. Later, in section 4.4, it will be evident that a reduction in heat coming down to the surface is dominating the cooling after a volcanic eruption (C1), and by this we mean that a decrease in SW_{net} (= SW_{down}-SW_{up}) + LW_{down} is larger than a decrease in LW_{up} + LE + SH (the heat emitted by the ocean).

In Figure 4.15 the change in fluxes are illustrated by making a simplified energy budget scheme where imbalances in the system are obvious, hence cooling. The fluxes that increase are colored red, while fluxes that decrease are colored blue. The length of the arrows indicates the size of the anomalies during a cooling event. A priori we had expected that the large release of aerosols into the strato-

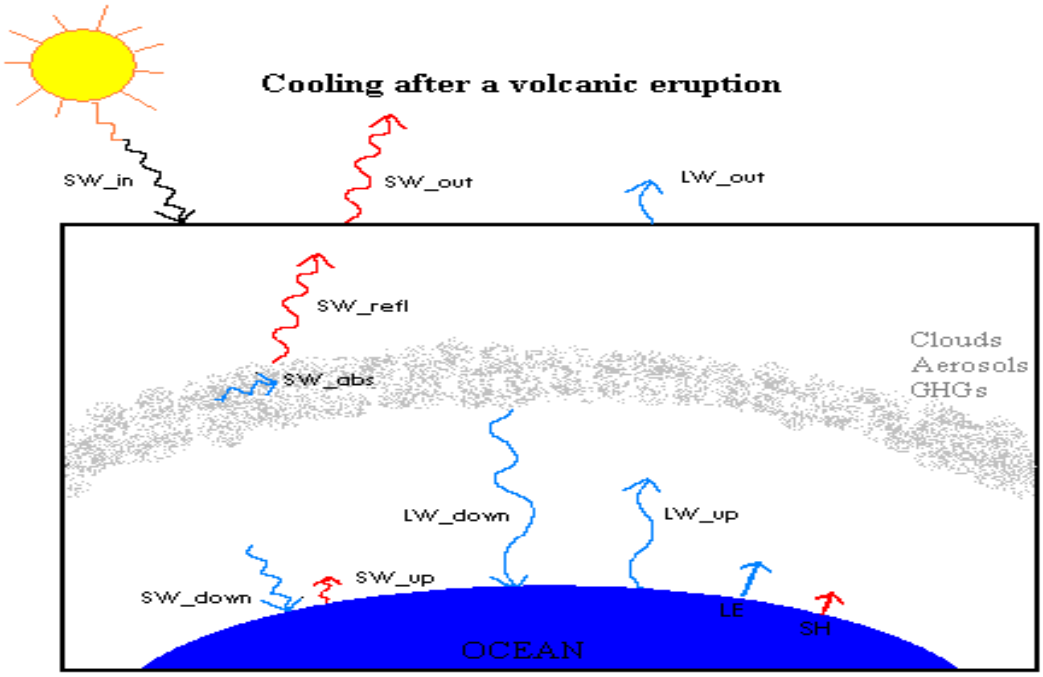

Figure 4.15: *Changes in surface energy fluxes during a cooling of the ocean heat content after a volcanic eruption. The fluxes at the surface are over ocean only, while the fluxes at the top of the atmosphere and in the atmosphere are globally. The length of the arrows indicates the size of the anomalies and not actual values. Blue arrows indicate a decrease while red arrows indicate an increase.*

sphere as a consequence of volcanic eruptions would have caused more reflection of SW radiation and therefore less SW radiation reaching the ocean (which are

both evident), resulting in ocean cooling. This is only partly true. It turns out that the largest decrease is in LW_{down}. But as we mentioned at first, a reduction in LW_{down} is a consequence of a decrease in the absorption of SW radiation and in the emission of LW radiation and LE from the ocean. A reduction in LW_{down} is therefore related to a reduction in both SW_{down} (indirectly) and SW_{abs} (directly). SW_{abs} is decreasing as a result of a great reflection of SW radiation in the atmosphere by volcanic aerosols and because SW radiation is mostly scattered rather than absorbed by these aerosols since they are not particularly large in size. The decrease in LW_{up} and LE are much greater than the decrease in SW_{down} and SW_{abs}. Since these fluxes have a greater decrease they contribute more to the decrease in LW_{down} than the decrease in transmitted or absorbed SW radiation. And since SW_{up} has a small increase, the absorption of SW radiation by the ocean is even less. The increase in SW_{up} is because the albedo of the ocean surface increases due to an increase in sea ice concentration (Figure 4.16(a)) as a result of a decrease in surface air temperature and sea surface temperature (Figure 4.17). When there is a cooling in the ocean, the surface air temperature over ocean is decreasing more than the sea surface temperature, hence a decrease in evaporation of the ocean. This explains why LE is also decreasing since LE is lost to the atmosphere through an evaporation. We can also see that the water vapor content (Figure 4.16(b)) is decreasing which is also a result of less evaporation (explained in section 2.1, equation 2.6). SH increases during a cooling which is due to a change in the difference between the air and ocean temperatures (equation 2.7): the air temperature gets colder than the sea surface temperature (Figure 4.17) which results in a greater exchange of heat from the ocean to the air above.

In the figures for the different fluxes (Figure 4.13 and 4.14) the longwave radiation coming down to the surface has the greatest anomalies during the 20th century, hence the most significant contribution to changes in the ocean. This is very clear in the beginning of the time series, but after approximately 1960 the anomalies for net downwelling shortwave radiation (SW_{net} = SW_{down}-SW_{up}) have a larger impact than earlier since it is now as big as or even bigger than LW_{down}. Since SW radiation first goes through the atmosphere where it is absorbed or transmitted directly down to the surface, it is logical that changes in SW_{down} occur earlier than changes in LW_{down}, as we mentioned at first. During the whole 20th century, LW_{down} has a positive trend while SW_{net} has a negative trend. Is SW_{net} sometimes dominating over LW_{down}? In Figure 4.13 for CCSM3 there is a cooling in the ocean around 1970 where SW_{net} has a greater decrease than LW_{down}, and the decrease also lasts a bit longer than LW_{down}. There is also a greater decrease in SW_{net} than LW_{down} around 1980 that dominates the cooling in the upper ocean. For Gfdl CM2.0 (Figure 4.13) there is a clear cooling in the OHC and a larger decrease in SW_{net} than in LW_{down} right after 1960. When SW_{net} dominates over LW_{down} it is referred to as global dimming as mentioned earlier, i.e. aerosols

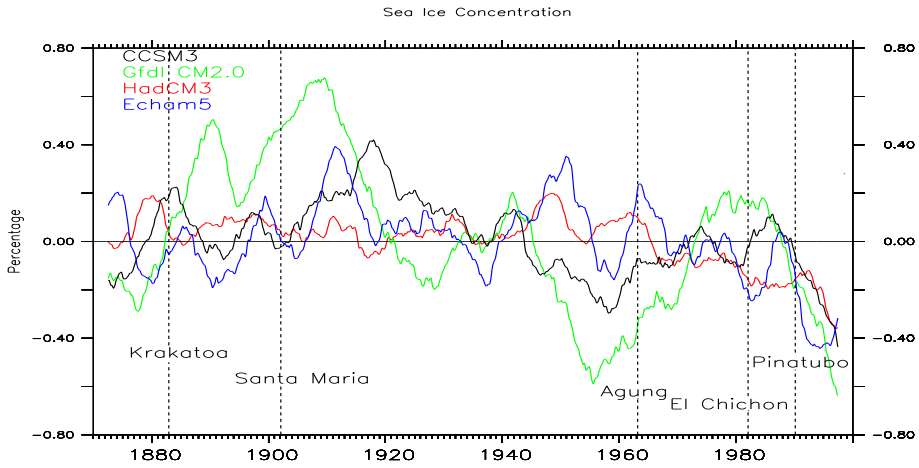

(a) Sea Ice Concentration

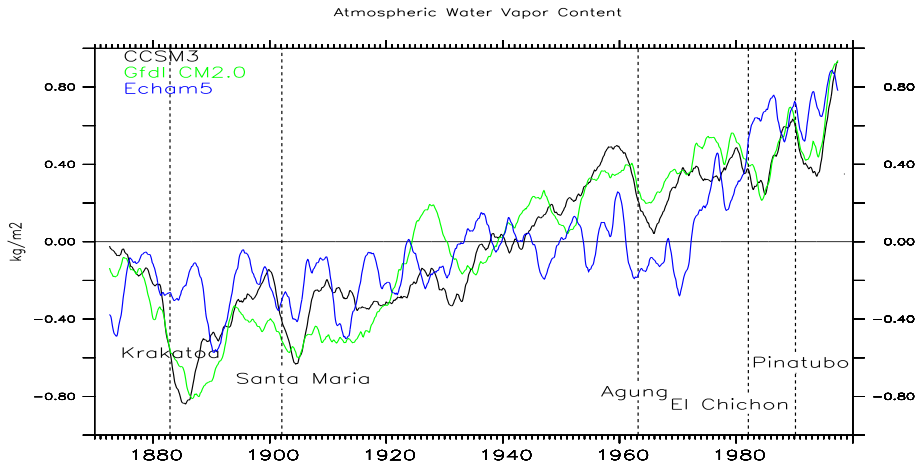

(b) Water Vapor

Figure 4.16: *a) Globally averaged sea ice concentration (anomalies), and b) Globally averaged water vapor content in the atmosphere (anomalies). The water vapor content for HadCM3 was not available in the IPCC's dataset catalogues (https://esg.llnl.gov:8443/), so this is why it is not in the figure. The anomalies are relative to 1870-1999.*

(natural and anthropogenic) shut out more of the incoming solar radiation which results in a cooling at the surface. But for the non-V models, which will be evident in Figure 4.19 and 4.20 in Case 3), LW_{down} usually dominates the cooling in the upper ocean.

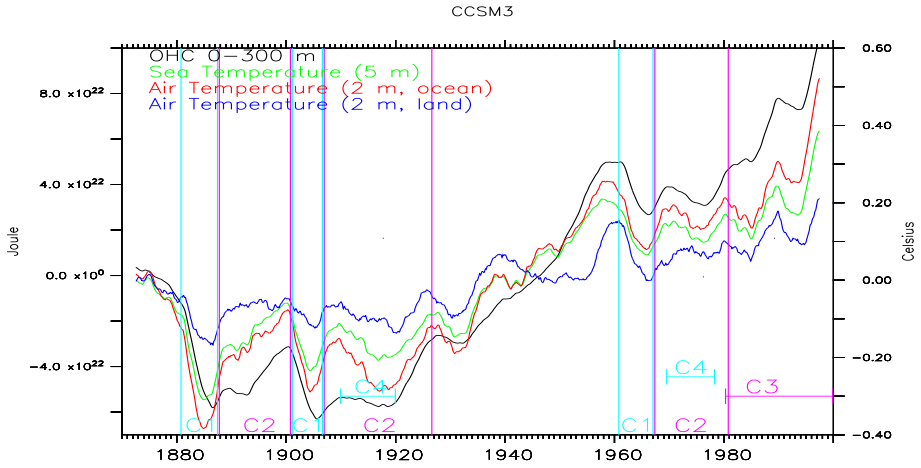

(a) CCSM3

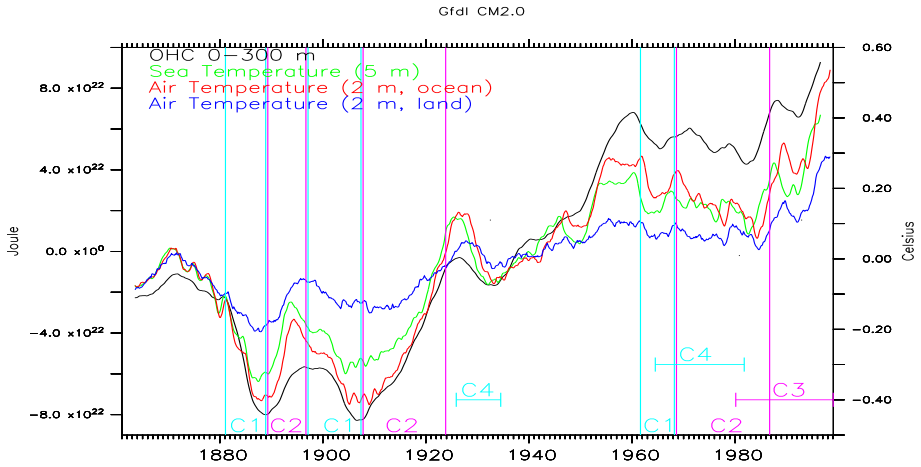

(b) Gfdl CM2.0

Figure 4.17: *V-models: Ocean heat content in 0-300 m, sea temperature in 5 m and air temperature in 2 m (anomalies). The anomalies for CCSM3 are relative to 1870-1999, and for Gfdl CM2.0 relative to 1861-2000.*

4.3.5 Case 2) Recovery after a volcanic eruption

Eventually, after some time, the stratospheric aerosols from a volcanic eruption will fall down into the troposphere where they will be carried to the surface by precipitation (Le Treut et al., 2007, IPCC). We will now investigate how the V-models (CCSM3 and Gfdl CM2.0) recover after a volcanic eruption. In this case we had expected that the SW radiation reaching the ocean surface would increase in

strength and therefore the ocean would start warming, but once again, the route is more complicated. If we look at the warming events (C2) in Figure 4.13 and 4.14, we can see that when the OHC starts to increase again, the fluxes that decreased in Case 1) will now increase and vice versa. We illustrate this in Figure 4.18 where blue arrows indicate a decrease, red arrows an increase and where the length of the arrows indicates the size of the anomalies.

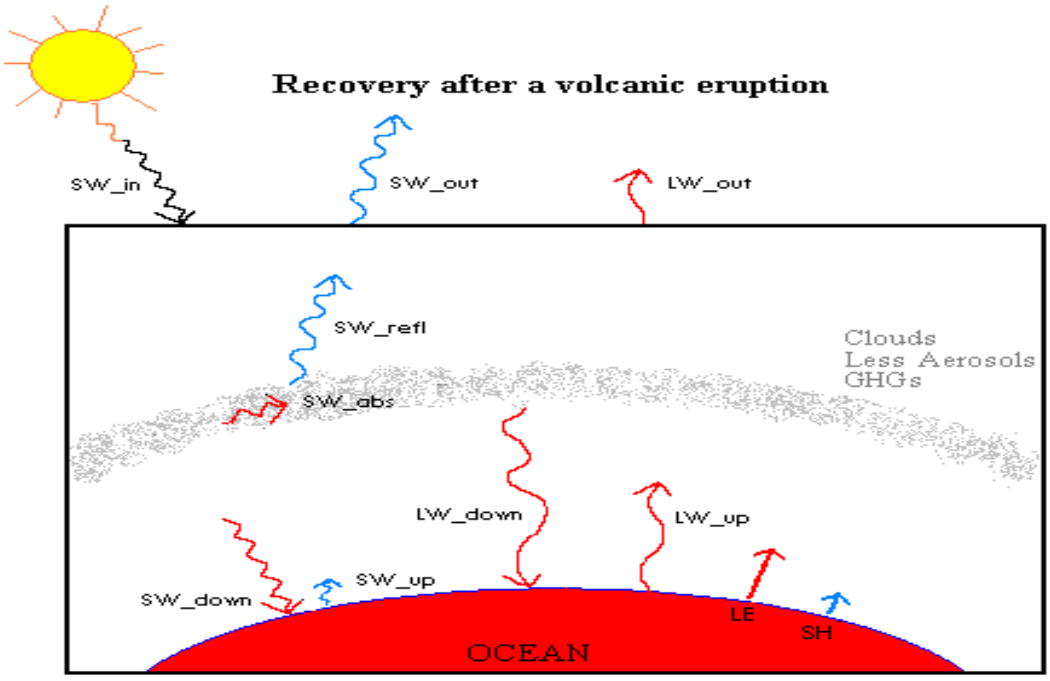

Figure 4.18: *Changes in surface energy fluxes during recovery of ocean heat content after a volcanic eruption. The fluxes at the surface are over ocean only, while the fluxes at the top of the atmosphere and in the atmosphere are globally. The length of the arrows indicates the size of the anomalies and not actual values. Blue arrows indicate a decrease while red arrows indicate an increase.*

By studying the figures for CCSM3 and Gfdl CM2.0 (Figure 4.13 and 4.14, respectively) we can see that a cooling in the upper ocean due to a volcanic eruption occurs very rapidly (steep curve) and only lasts for a few years. A recovery, on the other hand, is much slower, i.e. it takes a much longer time for the OHC to reach the value it had before the cooling started. But this is not always the case because sometimes there are new eruptions occurring before the OHC is fully recovered.

What we can see by studying Figure 4.18 is that LW_{down}, also in this case, is the most important factor in changing the ocean heat content, specifically it is more important than the increase in SW_{down}. When there are less aerosols in the

atmosphere, more of the radiation is transmitted through the atmosphere, hence an increase in SW_{down}. It is also obvious that SW_{down} is occurring before the other energy fluxes. There is an increase in the absorption of SW radiation. This is because the volcanic aerosols in the stratosphere eventually fall down to the troposphere and rain out which results in an increase in absorption of SW radiation rather than reflection. The increase in SW_{abs} is anyhow small compared to SW_{down} and the other fluxes, so it is not the main contributor to warming, but it is still very important and will contribute to the emission of LW radiation down to the surface along with absorbed LW radiation and LE release. The increase in SW_{down} will heat the ocean which results in an increase of LW_{up} and LE, and hence LW_{out} at the top of the atmosphere (which is also due to an increase in SW_{abs}). The water vapor content (Figure 4.16(b)) is also increasing which can explain the increase in LE because when the ocean is heated through an increase in downwelling radiation, the ocean starts to evaporate which results in more LE and hence more water vapor. Due to a large increase in downwelling SW and LW radiation, the sea ice concentration (Figure 4.16(a)) is reduced and consequently SW_{up} is decreasing. SH is decreasing due to a greater increase in the air temperature than the sea surface temperature which results in a reduction of heat exchange between the air-sea interface.

We can also see in Figure 4.17 that the air temperature over ocean starts to increase before the ocean heat content starts to increase after a volcanic eruption in CCSM3, but in Gfdl CM2.0 they occur approximately at the same time. So in Gfdl CM2.0 a warming in the atmosphere and ocean happens at exactly the same time, while for CCSM3 a warming happens first in the atmosphere then in the upper ocean. It is also evident that sometimes during the 20th century the air temperature over land changes after the air temperature over ocean does, and that the anomalies for the air temperature over land are less significant compared to the air temperature anomalies over ocean. This is logical because of the large heat capacity of the ocean.

All these changes in the surface energy fluxes in a recovery after a volcanic eruption are the opposite of what they are in a cooling after a volcanic eruption: the fluxes that increase in a warming, decrease in a cooling and vice versa. Despite this, there is one thing that separates the two cases: a cooling in the ocean due to a volcanic eruption happens very rapidly while a recovery is quite slow which we mentioned at first. This makes sense: cooling at the ocean surface is dynamically unstable, i.e. colder water is denser and could therefore tend to sink, whereas warming at the surface will simply cause stronger and more stable ocean stratification. It is therefore much harder to force a heating signal than a cooling signal into the deep ocean. If we look at Figure 4.13 and 4.14 we can see that after Krakatoa (1883) when the ocean starts to heat again, the value that the OHC had before the cooling started is not reached until the Santa Maria eruption in 1902

breaks out and causes a cooling again in the upper ocean. When the ocean starts to recover, there is a significant increase in the OHC to the early 1960s due to the increase in solar radiation and because the volcanic activity is very small. After the Agung eruption in 1963 a recovery is not complete until after 1980 due to the eruption of El Chichon in 1982 as well as the maximum amount of anthropogenic aerosols reached in the 1980s. This is evident for both CCSM3 and Gfdl CM2.0. The increase after 1980 is mostly due to the significant increase in greenhouse gases which started in the middle of the 20th century even though there was a powerful eruption of Pinatubo in 1991. But this can also be due to the decline in anthropogenic aerosols from the 1980s. The Pinatubo eruption does not affect the ocean as much as earlier eruptions did due to the warming by greenhouse gases. We will study this further in Case 3) where we will investigate the V-models and the non-V models.

4.3.6 Case 3) Warming due to greenhouse gases

A priori we had expected that the greenhouse gas warming, that increased significant in the middle of the 20th century, would induce a large increase in the ocean heat content earlier than what is evident. Due to major volcanic eruptions which eject sulphate aerosols into the stratosphere and due to a significant increase in anthropogenic aerosols, this warming is delayed in the V-models. In the non-V models, however, the significant increase starts earlier, in the late 1960s. We will therefore study how warming due to greenhouse gases, even though there is an increase in anthropogenic aerosols until the 1980s, appears in models with or without volcanic forcing. In Figure 4.5 and 4.6 (temperature contour plots) we found that the V-models started to heat up much earlier than the non-V models (Figure 4.7 and 4.8), but the increase in OHC (0-300 m) is evident even earlier. The increase in the V-models from approximately 1906 until the early 1960s is due to a recovery after the major volcanic eruptions in 1883 and 1902 along with the significant increase in incoming solar radiation as well as a small volcanic activity during this period of time. After 1960 this increase is paused until the early 1980s due to two more volcanic eruptions occurring in 1963 and 1982 and a significant increase in anthropogenic aerosols (maximum in the 1980s). After the latter eruption, the OHC starts to increase again as a response to the significant increase in greenhouse gases and due to a decline in anthropogenic aerosols, even though there is one major eruption of Pinatubo in 1991 (almost as great as Krakatoa) which otherwise would have caused a great cooling in the ocean.

In Figure 4.19 and 4.20 we have pointed out the period for warming due to greenhouse gases from approximately year 1969 (C3) for the non-V models. The flux anomalies for HadCM3 are almost on the same size as Echam5, and the LW radiation at the surface has the largest anomalies which was also the case for the

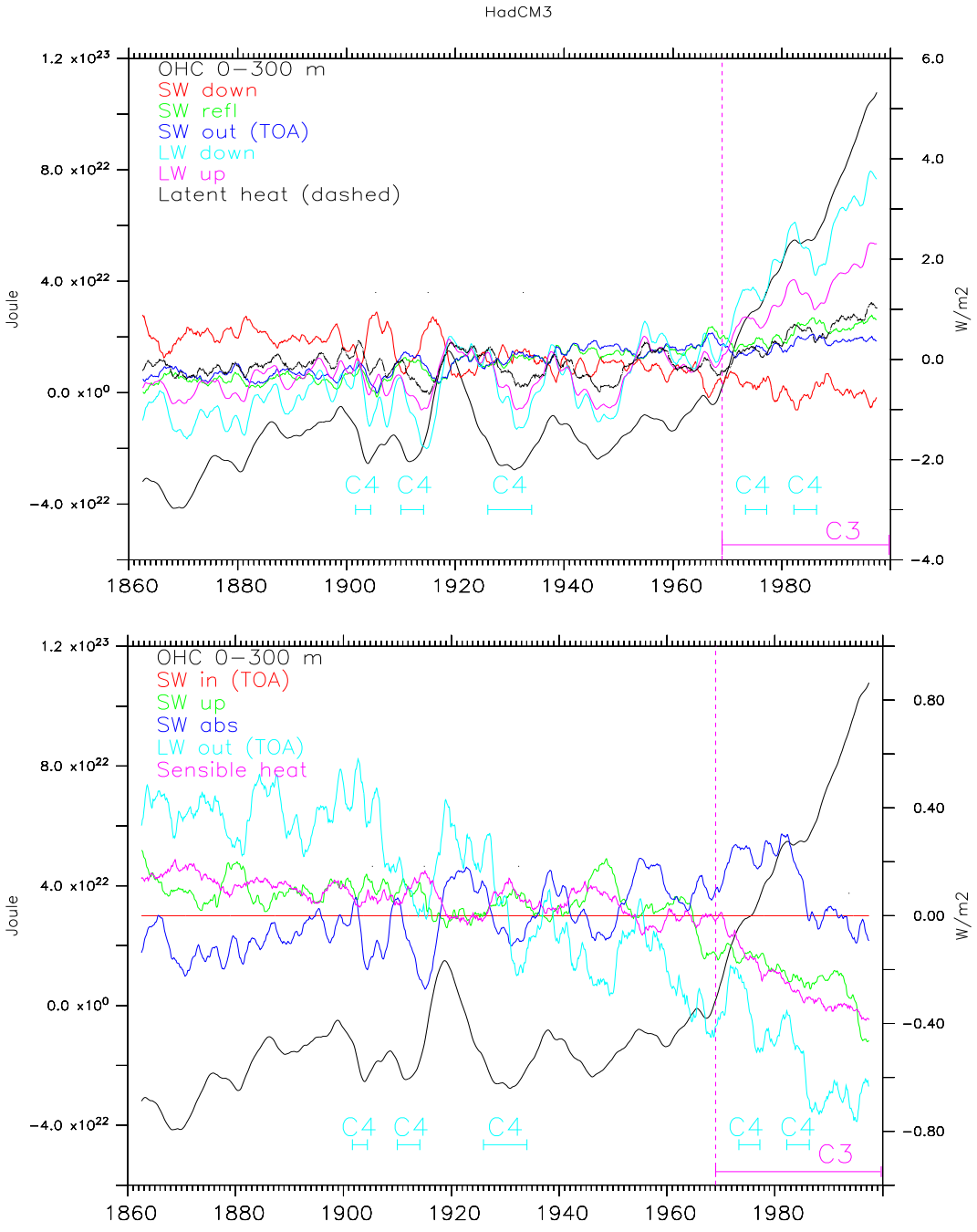

Figure 4.19: *Ocean heat content (0-300 m) and different energy fluxes in HadCM3 where the surface fluxes are over ocean only and the rest are global. (Upper) Flux components with the largest anomalies and (Lower) Flux components with the smallest anomalies. (Left y-axis: OHC; right y-axis: energy fluxes)*

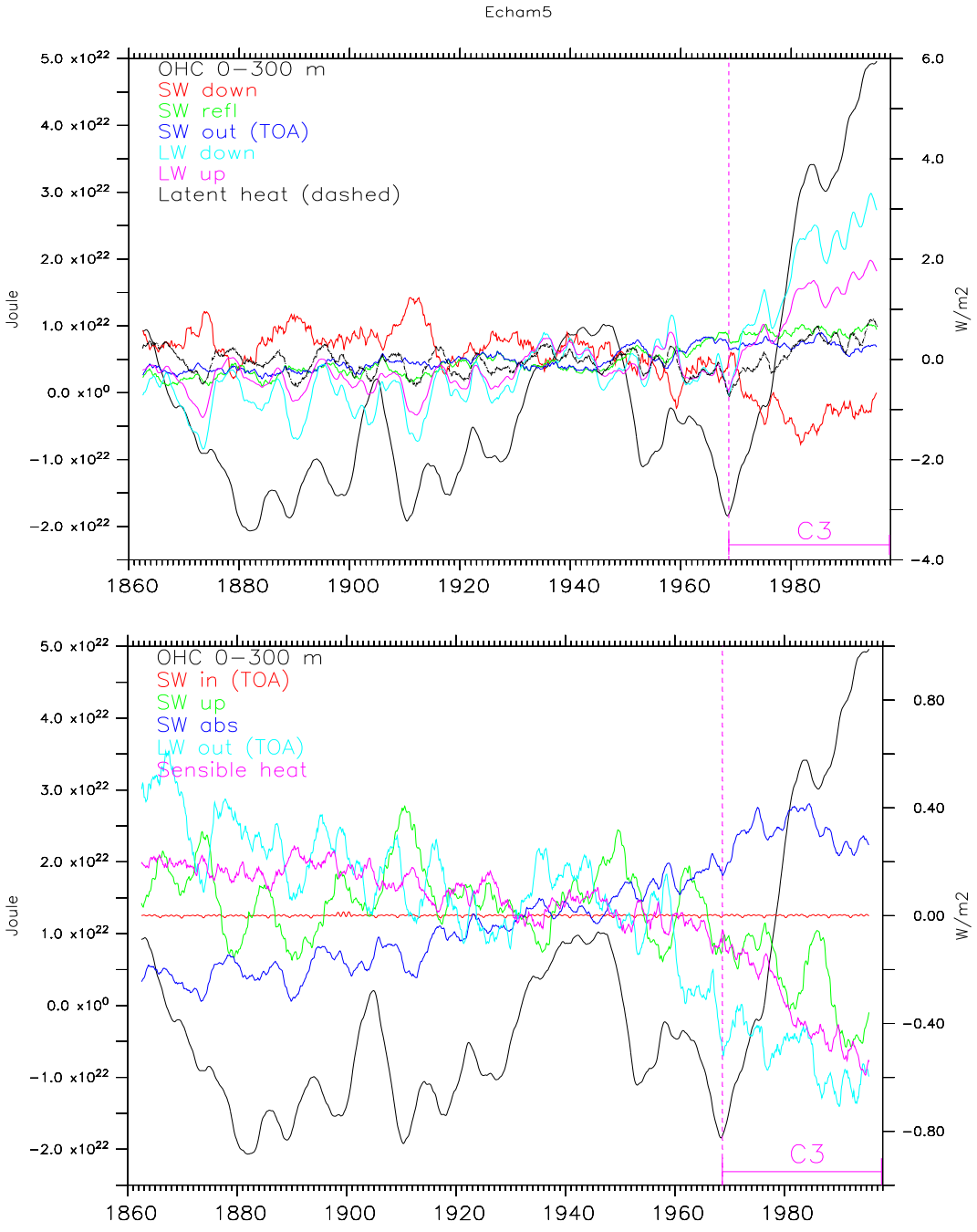

Figure 4.20: *Ocean heat content (0-300 m) and different energy fluxes in Echam5 where the surface fluxes are over ocean only and the rest are global. (Upper) Flux components with the largest anomalies and (Lower) Flux components with the smallest anomalies. (Left y-axis: OHC; right y-axis: energy fluxes)*

V-models in the previous cases. During the whole 20th century the variations in energy fluxes for the non-V models are somewhat different from the variations in the OHC, whereas for the V-models the energy fluxes were quite close to the variations in OHC. Despite this, it is obvious that when a flux throughout the whole 20th century has a positive (negative) trend for CCSM3 and Gfdl CM2.0 it also has a positive (negative) trend for HadCM3 and Echam5. One clear difference between the V-models and the non-V models is that the incoming solar radiation anomalies are almost a straight line (red) in Figure 4.19 and 4.20 which is simply because the non-V models do not have variations in the solar forcing (see section 3.1). For the non-V models there is no evidence of SW_{net} dominating a cooling in the ocean over LW_{down} as was evident for the V-models in Case 1).

Even though the trends of the energy fluxes are similar for all the models, the sizes of the anomalies are somewhat different. Because of this we decide to separate the models into two figures which show the energy budget of the Earth, shown in Figure 4.21(a) for the non-V models and Figure 4.21(b) for the V-models.

Water vapor is the most important greenhouse gas. The periods for warming due to greenhouse gases introduced here show that the water vapor content in the atmosphere (Figure 4.16(b)) has increased significantly for CCSM3, Gfdl CM2.0 and Echam5 (the water vapor content was not available for HadCM3). Because of the significant increase in water vapor content after 1960 which is a consequence of heating due to the increase in other greenhouse gases, especially CO_2, the greenhouse effect is enhanced which results in a further warming of the climate system, especially after 1980 when the anthropogenic aerosols declined.

In Figure 4.21(a), LW_{down} and LW_{up} are still the dominating fluxes and are increasing significantly which is due to a large amount of absorption in the atmosphere by greenhouse gases. SW_{abs} behaves differently from the other fluxes: it is increasing until the early 1980s and then decreasing. The trend for SW_{down} is not easy to see for HadCM3, but for Echam5 it is the opposite of SW_{abs} (decreasing first, then increasing). This is most likely due to the decay of anthropogenic aerosols from the early 1980s. Due to global dimming (mentioned in section 2.1), there has been an overall decrease in SW_{down} during the 20th century, but in this period (1969-1999) there is no specific trend. There is no significant changes in the outgoing solar radiation for the non-V models as well, during this period. Otherwise, the trends are quite clear: LW_{out}, SW_{up} and SH are decreasing while SW_{refl} and LE are increasing. LE has the next biggest anomalies compared to the LW radiation at the surface. This means that when there are only variations in the anthropogenic forcing and no volcanic forcing included as well as no solar variability, it will result in a heating of the climate system where LE together with the LW radiation at the surface dominate the heating. Even though the reflection of SW radiation is slightly increasing, which is due to anthropogenic aerosols, there

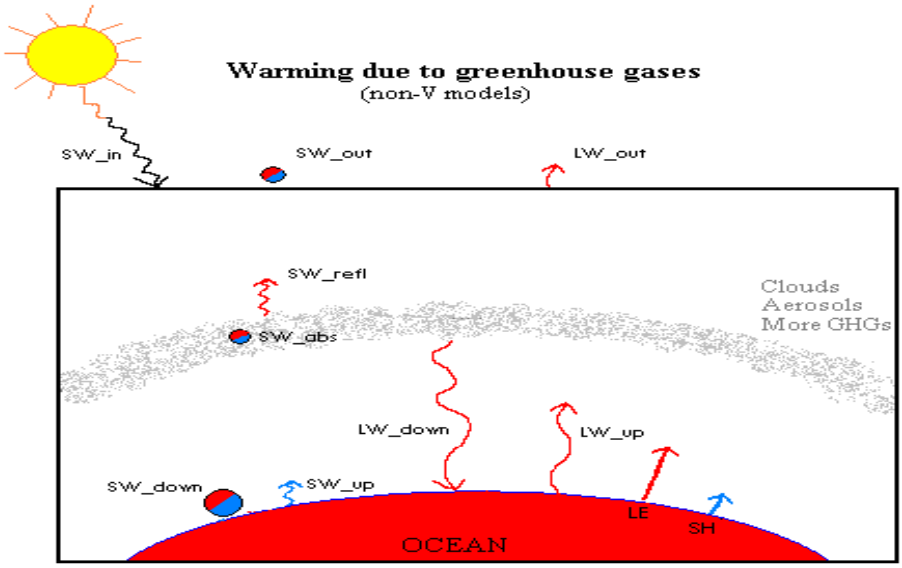

(a) Non-V models

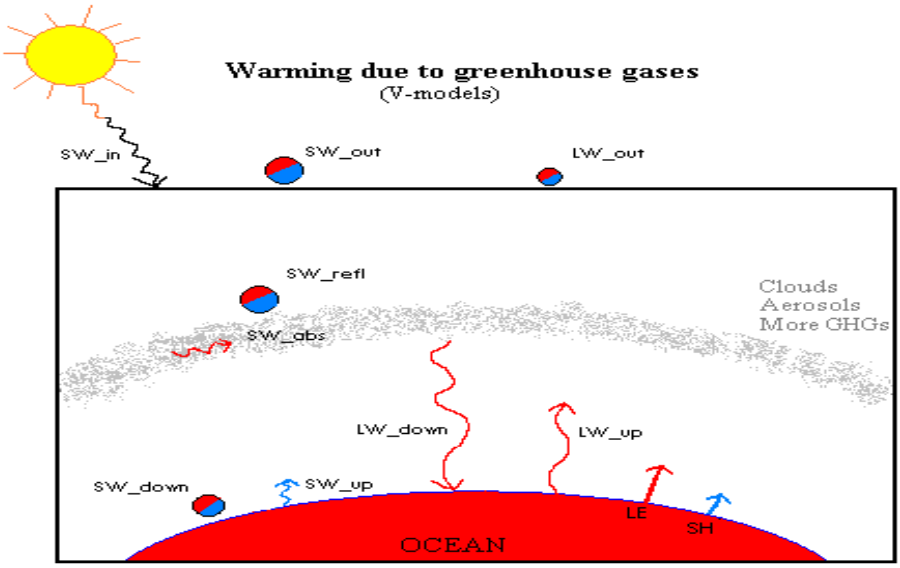

(b) V-models

Figure 4.21: *Surface energy fluxes during warming of the ocean heat content due to greenhouse gases for: a) Non-V models; b) V-models. The fluxes at the surface are over ocean only, while the fluxes at the top of the atmosphere and in the atmosphere are globally. The length of the arrows indicates the size of the anomalies and not actual values. Blue arrows indicate a decrease while red arrows indicate an increase. The circles with red and blue color indicate no specific trend, but that there are variations, both increase and decrease, during the specified period.*

will still be heating of the climate system from the late 1960s, regarding the non-V models.

In Figure 4.21(b) for the V-models are LW_{down} and LW_{up} also the fluxes that dominate. SW_{refl}, SW_{out} and SW_{down} have the next largest anomalies. SW_{down} has no significant trend during this period, as well as SW_{refl}, SW_{out} and LW_{out}. The only thing that is evident in these fluxes are the volcanic eruptions, but this do not affect the ocean as much, like it did in Case 1). It is also obvious that the LW radiation at the surface is not as much affected by the eruptions which is logical since volcanic aerosols reflect radiation rather than absorb it. SW_{abs} is increasing which contributes to the increase in LW_{down}. In Delworth et al. (2005) both natural and anthropogenic aerosols contribute to a delay of ocean warming that solely occurs from increasing greenhouse gases. This is also what we have found here: after around 1960 there is a delay in the ocean heat content increase for CCSM3 and Gfdl CM2.0, and the warming do not continue until after 1980. When there are both variations in natural and anthropogenic forcing (V-models), LW_{down} will dominate the heating, hence the heating is due to a greater emission down to the ocean as a consequence of an increase in SW_{abs}, LW_{up} and LE which contribute to a larger emission of LW_{down}.

Anthropogenic aerosols were at its maximum in the 1980s and therefore there should not be an increase until after the aerosols declined, but as we can see the non-V models started to increase earlier than this. The V-models, on the other hand, started to increase after 1980. Since the latter two models also include volcanic forcing as well as anthropogenic forcing, the volcanic aerosols must be more important in cooling the climate system than the anthropogenic aerosols.

During the 20th century, the upwelling LW radiation from the surface has increased in all the models. This is in connection with the fact that the OHC has increased. When the ocean is heated, it results in an greater emission of energy. SW radiation down at the surface has decreased during the 20th century for all the models. This could either be in connection with that more is absorbed in the atmosphere, which results in more emissions of LW radiation down or up, or that more is reflected due to an increase in aerosols (both anthropogenic and natural) referred to as global dimming (mentioned in section 2.2). For the V-models the absorption of SW radiation in the atmosphere has increased which is due to an increase in incoming solar radiation and due to a greater amount of greenhouse gases. LW_{out} has slightly decreased for all the models, especially for the non-V models. This is why the climate system is heating because the absorption of SW radiation is resulting in a greater emission of downwelling LW radiation to the surface since the outgoing LW radiation has decreased. Even though downwelling SW radiation has decreased in the V-models, which could have resulted in a decrease of the OHC, the increase in downwelling LW radiation is so large that we still believe that LW_{down} is the main contributor to the increase in

ocean heat content. But wether this increase is due to an increase in heat release from the ocean or due to an increase in SW absorption and downwelling SW radiation is a question which will be investigated further in the next section.

4.4 Cooling or warming originating in the ocean

In all the cases we have studied so far the ocean cooling or warming is caused by changes in the atmospheric composition which alters the energy fluxes. In the previous cases SW_{down} is always occurring first and is responsible for changes in the other fluxes. The other fluxes occur at approximately the same time. A priori we had expected the ocean to set its own timescales to modulate climate as a consequence of its own natural variability. Here we look for evidence of such events.

We will investigate this by comparing the heat released from the ocean ($HEAT_{up}$) to the heat coming down to the ocean ($HEAT_{down}$) which is illustrated in Figure 4.22 for the V-models and in Figure 4.23 for the non-V models where the events are marked by C4. The heat coming up from the ocean is the sum of LW_{up}, LE and SH, while the heat coming down to the ocean is the sum of SW_{net} and LW_{down}. If $HEAT_{up}$ is decreasing more than $HEAT_{down}$ during a cooling, this simply means that the cooling is a response of less energy released from the ocean rather than less energy emitted down to the ocean. From the previous cases the air temperatures over ocean follows the ocean heat content well for the V-models (see Figure 4.17), so that a cooling or warming in OHC is also evident in the atmosphere.

If we look at Figure 4.22(a) for CCSM3 we can see that when there is a cooling around 1910 to 1920, $HEAT_{up}$ is bigger in change than $HEAT_{down}$. This is also occurring around 1970 to 1977. So in CCSM3 we have two occurrences where the cooling starts in the ocean. In Figure 4.22(b) for Gfdl CM2.0 there is obvious an occurrence of cooling starting in the ocean around 1925 to 1935, and also from around 1967 to 1982 (the cooling is not evident in the ocean until 1971). If we look at Figure 4.23(a) for HadCM3 we can see that there are several small coolings in the ocean where $HEAT_{up}$ dominates over $HEAT_{down}$: there are some occurrences in the period from 1910 to 1920, one from 1919 to 1931, one from 1974 to 1977 and one from 1982 to 1986. For the last two occasions a significant cooling in the ocean is not evident, but anyhow $HEAT_{up}$ is dominating over $HEAT_{down}$.

Echam5 in Figure 4.23(b) stands out compared to the other models. It is clear that $HEAT_{up}$ dominates over $HEAT_{down}$ almost during the whole 20th century. In the other models it is usually less energy received by the ocean at the air-sea interface that dominates the cooling, not actually loss from the ocean. Because of this we can not fully trust Echam5. The other three models are more reliable since

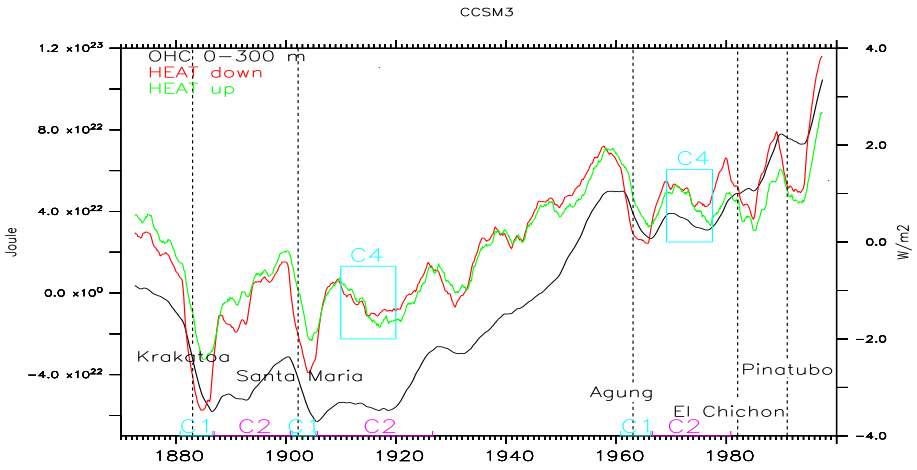

(a) CCSM3

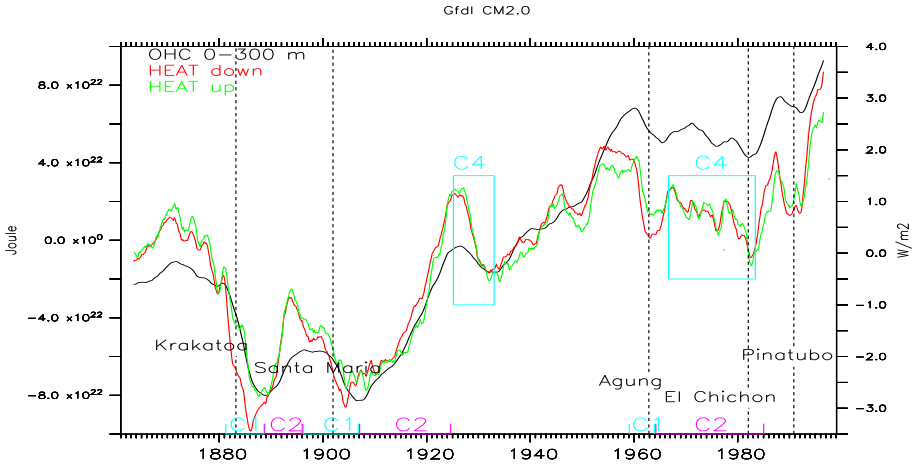

(b) Gfdl CM2.0

Figure 4.22: *Ocean heat content (0-300 m), downwelling energy over ocean ($SW_{net}+LW_{down}$) and upwelling energy over ocean ($LW_{up}+LE+SH$) for a) CCSM3, and b) Gfdl CM2.0. The anomalies are relative to 1870-1999 for CCSM3 and 1861-2000 for Gfdl CM2.0. (Left y-axis: OHC; right y-axis: $HEAT_{down}$ and $HEAT_{up}$)*

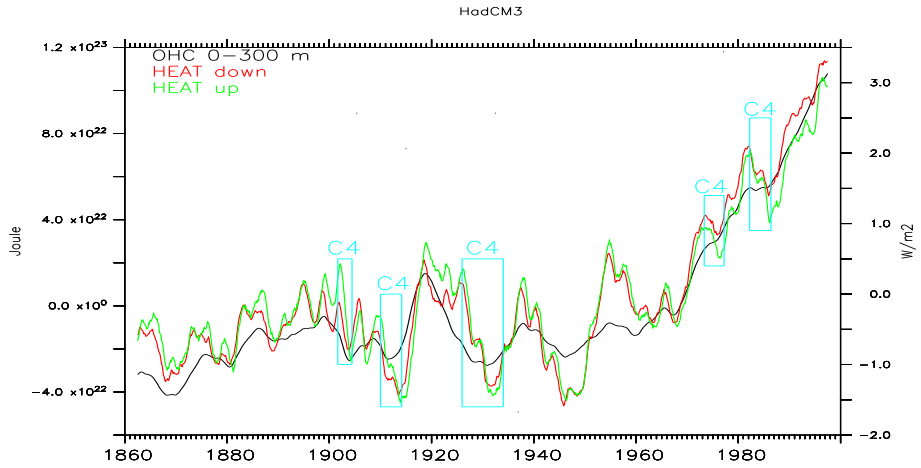

(a) HadCM3

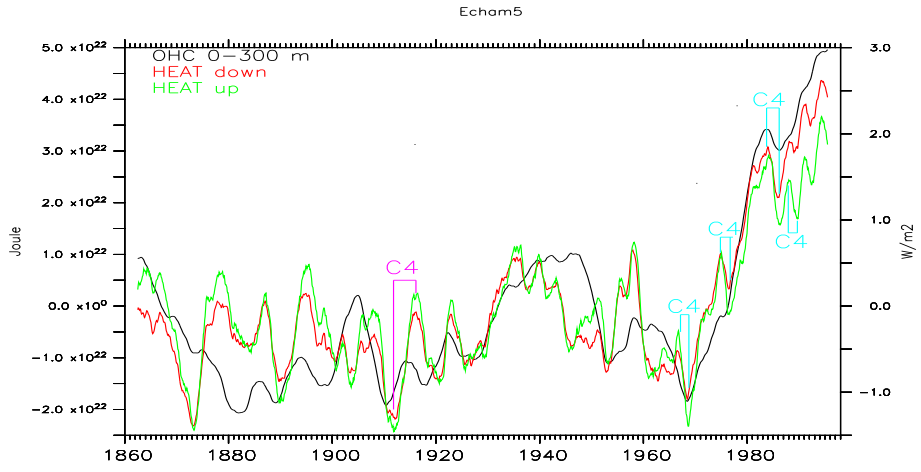

(b) Echam5

Figure 4.23: *Ocean heat content (0-300 m), downwelling energy over ocean ($SW_{net}+LW_{down}$) and upwelling energy over ocean ($LW_{up}+LE+SH$) for a) HadCM3, and b) Echam5. The anomalies are relative to 1860-1999. (Left y-axis: OHC; right y-axis: $HEAT_{down}$ and $HEAT_{up}$)*

they only have a few occurences of domination in cooling by the ocean. We can also see that when the cooling is dominated by the ocean, it lasts much longer in CCSM3, Gfdl CM2.0 and HadCM3 than in Echam5.

In section 4.2 there were two warming events evident in the ocean for the non-V models that were not evident in the atmosphere until a few years later. Was this warming in the ocean causing a warming in the atmosphere? For HadCM3 this warming event occurred in the atmosphere at approximately year 1918, while it was evident in the ocean at a depth of 200-300 m in approximately five years earlier (see Figure 4.7). In Figure 4.23(a) for HadCM3, $HEAT_{up}$ is dominating over $HEAT_{down}$ from 1913 to 1920 as we expected. In Figure 4.8 for Echam5 a warming is evident from 1929 in the ocean at a depth of 100 m while in the atmosphere the warming is not evident until 1932. Figure 4.23(b) shows that $HEAT_{up}$ dominates over $HEAT_{down}$ from 1929 to 1936. No such warming events were evident in the V-models in section 4.2, but despite this, we choose to study if such warming events are evident in Figure 4.22. For CCSM3 there are two occurrences where $HEAT_{up}$ dominates over $HEAT_{down}$ even though this was not evident in section 4.2, and that is approximately in 1920-1926 and 1950-1958. Gfdl CM2.0 has no such obvious warming events.

In section 4.1, when we compared OHC in 0-300 m with observations from Domingues et al. (2008) as well as the comparison of global surface air temperatures, we found that all the models were relatively realistic after 1970. We then also assume that we can rely on the energy fluxes being realistic for this period of time. By the detections we made here, we can conclude that the ocean sometimes is responsible for a cooling in the climate system. The periods where this is evident are: around 1970-1980 for CCSM3, around 1965-1980 for Gfdl CM2.0, around 1974-1977 and 1982-1986 for HadCM3, and several occasions for Echam5 (1967-1969, 1975-1977, 1984-1986 and 1988-1990).

Chapter 5

Summary and conclusion

We have now investigated four coupled climate models from the IPCC's model runs of the climate 20th century experiment (20C3M). Two of the models investigated had variations in both natural and anthropogenic forcing (CCSM3 and Gfdl CM2.0, referred to as the V-models) while the two others had only variations in the anthropogenic forcing (HadCM3 and Echam5, referred to as the non-V models) as seen in Table 3.2 (section 3.1). We have performed both qualitative and quantitative analysis of temperatures in the atmosphere and in the ocean. The models were found to be relatively realistic by comparing them with observations of ocean heat content (0-300 m) and surface air temperature. Our purpose with this investigation was to locate ocean heat release and uptake and how this influence the climate system of the Earth during the 20th century. We did this by studying the changes in energy fluxes during cooling and warming periods and discussed which factors (greenhouse gases, natural and anthropogenic aerosols, and solar variability) were responsible for these changes.

In section 4.1 we investigated how realistic the models are by comparing them to observations of ocean heat content in 0-300 m and surface air temperature (global and land). Sometimes CCSM3 and Gfdl CM2.0 (with natural and anthropogenic forcing) were better than HadCM3 and Echam5 (anthropogenic forcing only), and in other periods they were worse. The V-models had good agreement in the magnitude of observed and simulated decadal variability while the non-V models did not reproduce the decadal variations. Overall, the models reproduced the ocean heat content and the surface air temperature quite well. We could therefore continue our study on the basis that the models were relatively realistic.

We could not perform an exact energy budget for the models since a calculation of the ocean heat content from the surface net energy flux resulted in much greater values than for the volume integrated potential temperatures in the ocean (the latter method is the method we have used to compute the ocean heat content in this thesis). This means that there was an imbalance in the models energy bud-

get in addition to the general drift that all the models experience at depth. Despite all of this, we could tell from Figure 4.9 and 4.10 that there was a close connection between the ocean heat content in 0-300 m and the surface net energy flux. In addition, we knew that the models were close to the observations, and by all this we still felt satisfied to continue our study.

Volcanic forcing has been much more important to the 20th century than the few episodes should indicate. That is because of the asymmetry between heating and cooling of the ocean: the cooling events reach deeper and keep the atmosphere cold for a longer time than a priori expected (2-3 years). This can probably explain the relatively low global average temperatures from 1880-1940 in Figure 4.3(a). Heating at the ocean surface results in a stronger and more stable ocean stratification, and is therefore much harder to force into the deep ocean than a cooling signal. This explains why the system sometimes did not fully recover until the next volcanic eruption appeared which was evident after the Krakatoa eruption in 1883 where a recovery was not completed before the Santa Maria volcano had an eruption.

Recent volcanic events have been less powerful in cooling the Earth for a prolonged period of time, possibly because the ocean stratification is much stronger now due to the heating in the late 20th century as a response to anthropogenic forcing, i.e. an increase in greenhouse gases and a decrease in anthropogenic aerosols (after 1980). In the late 19th and early 20th century, the ocean was drastically cooled by two major volcanic eruptions (Krakatoa in 1883 and Santa Maria in 1902). The recovery from this significant cooling endured until the early 1960s as a response to the increase in incoming solar radiation and a very small volcanic activity (Hartmann, 1994). From thereon the increase in anthropogenic aerosols was significant until the 1980s along with two major volcanic eruptions in 1963 and in 1982 which resulted in a cooling of the ocean. If there were no volcanic eruptions or anthropogenic aerosols, a warming due to greenhouse gases would have caused warmer temperatures earlier than what is evident here. The Pinatubo eruption in 1991 was almost as powerful as the Krakatoa eruption in 1883 and in Figure 4.13 and 4.14 the reflection of incoming solar radiation is very large after this eruption while the decline in the ocean heat content is quite small. Because of this the warming, greenhouse gases must have a significant influence on the climate system along with the decay in anthropogenic aerosols from the 1980s. The increase in incoming solar radiation also had its impact on the significant warming to approximately 1960 (Hartmann, 1994, Figure 11.3), but not as much as the greenhouse gases had, especially not in the late 20th century (Forster et al., 2007, IPCC).

Even though the downwelling shortwave radiation at the surface decreases during the 20th century, the ocean warms. This is explained by a significant increase in downwelling longwave radiation as well as an increase in upwelling

longwave radiation from the ocean surface where the change during the whole century is larger than for the change in net downwelling shortwave radiation at the ocean surface. This implies that the ocean surface is receiving more energy from the longwave radiation, hence a warming. But what happens with the atmosphere when the ocean is heating? We found that an increase or a decrease starts almost at the same time in the atmosphere as in the ocean. This is logical since the incoming shortwave radiation is absorbed in the atmosphere and in the upper ocean which contributes to heating. Instead of studying the 20th century as a whole, we were only looking at short periods and found in Case 1) that the net downwelling shortwave radiation in some cases actually dominated cooling in the upper ocean by a larger decrease than the downwelling longwave radiation. This was evident for CCSM3 around 1970 and 1980 and for Gfdl CM2.0 right after 1960. For the non-V models the downwelling longwave radiation was usually dominating cooling and warming events, but the downwelling shortwave radiation was sometimes as large as the downwelling longwave radiation.

All the models show evidence of the ocean providing its own time scale and imposing a cooling signal on the atmosphere, however these events are not dominating the modeled 20th century climate. But from the comparison of modeled ocean heat content to observed ocean heat content, we found that CCSM3 and Gfdl CM2.0 followed the observations quite well from 1950 until 1999 while HadCM3 and Echam5 had a good fit with the observations from 1970 until 1999. The modeled surface air temperature was also reproduced quite well for all the models. Since the energy fluxes deviate as the ocean heat content does, we would assume that the variations in the different energy fluxes also agree with reality like the ocean heat content. Because of this we hypothesize that changes in energy fluxes are realistic and find that the ocean in some cases dominates a cooling in the climate system. From approximately year 1970, when the models reproduced ocean heat content well, we found that less energy from the ocean dominated a cooling around 1970-1980 for CCSM3, around 1965-1980 for Gfdl CM2.0, around 1974-1977 and 1982-1986 for HadCM3, and several occasions for Echam5 (1967-1969, 1975-1977, 1984-1986 and 1988-1990). Since we have consider the volcanic models to be most realistic, we can conclude that the ocean has been responsible for a cooling in the period of 1970 to 1980, which was also evident for HadCM3 (1974-1977) and for Echam5 (1975-1977). But mostly, it is changes in the composition of the atmosphere that are responsible for cooling or warming in the climate system according to the models we have studied here.

As a suggestion to further studies, the findings in this thesis could be investigated closer by performing statistical analysis such as a t-test in the comparison of simulated and observed ocean heat content as well as global surface air temperature. Further the energy fluxes could be studied closer by using a lag-lead correlation

between each flux for better understanding of the energy balance of the Earth. Also a more careful calculation of the ocean heat content can be performed and an investigation of regional changes in the ocean as well as in the energy balance to find out were the ocean releases and takes up heat. Another idea is to look at variations in cloud cover and how this influence the radiative forcing.

As the reader can see in this thesis, there are many factors that need to be investigated closer which is important and most of all very interesting!

List of Figures

Bibliography

Bindoff, N., J. Willebrand, V. Artale, A. Cazenave, J. Gregory, S. Gulev, K. Hanawa, C. L. Quéré, S. Levitus, Y. Nojiri, C. Shum, L. Talley, and A. Unnikrishnan (2007). Observations: Oceanic Climate Change and Sea Level. In: Climate Change 2007: The Physical Science Basis. Contribution of Working Group I to the Fourth Assessment Report of the Intergovernmental Panel on Climate Change [Solomon, S., D. Qin, M. Manning, Z. Chen, M. Marquis, K.B. Averyt, M. Tignor and H.L. Miller (eds.)], p. 389-393. Technical report, Cambridge University Press, Cambridge, United Kingdom and New York, NY, USA.

Broecker, W. S. (1997). Thermohaline Circulation, the Achilles Heel of Our Climate System: Will Man-Made CO2 Upset the Current Balance? *Science 278*, 1582–1588.

Delworth, T. L., V. Ramaswamy, and G. L. Stenchikov (2005). The impact of aerosols on simulated ocean temperature and heat content in the 20th century. *Geophysical Research Letters 32*, L24709, doi:10.1029/2005GL024457.

Domingues, C. M., J. A. Church, N. J. White, P. J. Gleckler, S. E. Wijffels, P. M. Barker, and J. R. Dunn (2008, June). Improved estimates of upper-ocean warming and multi-decadal sea-level rise. *Nature 453*, 1090–1093, doi:10.1038/nature07080.

Fioletov, V., G. Bodeker, A. Miller, R. McPeters, and R. Stolarski (2002). Global and zonal total ozone variations estimated from ground-based and satellite measurements: 1964-2000. *Journal of Geophysical Research 107*, 21–5, doi:10.1029/2001JD001350.

Forster, P., V. Ramaswamy, P. Artaxo, T. Berntsen, R. Betts, D. Fahey, J. Haywood, J. Lean, D. Lowe, G. Myhre, J. Nganga, R. Prinn, G. Raga, M. Schulz, and R. V. Dorland (2007). Changes in Atmospheric Constituents and in Radiative Forcing. In: Climate Change 2007: The Physical Science Basis. Contribution of Working Group I to the Fourth Assessment Report of the Intergovern-

mental Panel on Climate Change [Solomon, S., D. Qin, M. Manning, Z. Chen, M. Marquis, K.B. Averyt, M.Tignor and H.L. Miller (eds.)], p. 135-137, 163. Technical report, Cambridge University Press, Cambridge, United Kingdom and New York, NY, USA.

Gleckler, P. J., K. R. Sperber, and K. AchutaRao (2006, June). Annual cycle of global ocean heat content: Observed and simulated. *Journal of Geophysical Research 111*, C06008, doi:10.1029/2005JC003223.

Hansen, J., L. Nazarenko, R. Ruedy, M. Sato, J. Willis, A. D. Genio, D. Koch, A. Lacis, K. Lo, S. Menon, T. Novakov, J. Perlwitz, G. Russell, G. A. Schmidt, and N. Tausnev (2005). Earth's Energy Imbalance: Confirmation and Implications. *Science 308*, 1431–1435.

Hartmann, D. L. (1994). *Global Physical Climatology*, Volume 56 of *International Geophysics Series*, pp. 13, 23–25, 42, 71, 99–101, 290. Waveland Press, Inc.

Jacob, D. (1999). *Introduction to Atmospheric Chemistry*, pp. 115–116, 126–128, 131–132, 138–140, 146–154. Princeton University Press.

Jones, P. and M. Salmon (2008). Climatic Research Unit: Data. CRUTEM3 and HadCRUT3 at *http://www.cru.uea.ac.uk/cru/data/temperature/* (accessed April 2009).

Knauss, J. A. (1997). *Introduction to Physical Oceanography, second edition*, pp. 48–49. Waveland Press, Inc.

Le Treut, H., R. Somerville, U. Cubasch, Y. Ding, C. Mauritzen, A. Mokssit, T. Peterson, and M. Prather (2007). Historical Overview of Climate Change. In: Climate Change 2007: The Physical Science Basis. Contribution of Working Group I to the Fourth Assessment Report of the Intergovernmental Panel on Climate Change [Solomon, S., D. Qin, M. Manning, Z. Chen, M. Marquis, K.B. Averyt, M. Tignor and H.L. Miller (eds.)], p. 96-97, 100. Technical report, Cambridge University Press, Cambridge, United Kingdom and New York, NY, USA.

Levitus, S., J. Antonov, and T. Boyer (2005). Warming of the world ocean, 1955-2003. *Geophysical Research Letters 32*, L02604, doi:10.1029/2004GL021592.

Liepert, B. G. (2002). Observed reductions of surface solar radiation at sites in the United States and worldwide from 1961 to 1990. *Geophysical research letters 29*, 61–1 to 61–4, doi:10.1029/2002GL014910.

Liou, K. (2002). *An Introduction to Atmospheric Radiation* (Second ed.), Volume 84 of *International Geophysics Series*, pp. 65–78, 82–87, 116–122, 478. Academic Press.

Mauritzen, C. (1996). Production of dense overflow waters feeding the North Atlantic across the Grenland-Scotland Ridge. Part 2: An inverse model. *Deep-Sea Research I 43*, 810, 829.

Meehl, G., T. Stocker, W. Collins, P.Friedlingstein, A. Gaye, J. Gregory, A. Kitoh, R. Knutti, J. Murphy, A. Noda, S. Raper, I. Watterson, A. Weaver, and Z.-C. Zhao (2007). Global Climate Projections. In: Climate Change 2007: The Physical Science Basis. Contribution of Working Group I to the Fourth Assessment Report of the Intergovernmental Panel on Climate Change [Solomon, S., D. Qin, M. Manning, Z. Chen, M. Marquis, K.B. Averyt, M. Tignor and H.L. Miller (eds.)], p. 755-756. Technical report, Cambridge University Press, Cambridge, United Kingdom and New York, NY, USA.

NASA (2009). GISS: Global-mean monthly, annual and seasonal dTs based on met.station data. *http://data.giss.nasa.gov/gistemp/* (accessed March 2009).

Peixoto, J. and A. Oort (1992). *Physics of Climate*, pp. 308–309. American Institute of Physics.

Pickard, G. and W. Emery (1982). *Descriptive Physical Oceanography* (Fourth enlarged ed.)., pp. 35. Pergamon Press.

Ramanathan, V. and Y. Feng (2009). Air pollution, greenhouse gases and climate change: Global and regional perspectives. *Atmospheric Environment 43*, 37–50, doi:10.1016/j.atmosenv.2008.09.063.

Roderick, M. L. and G. D. Farquhar (2002). The cause of decreased pan evaporation over the past 50 years. *Science 298*, 1410–1411.

Santer, B., C. Mears, F. Wentz, K. Taylor, P. Gleckler, T. Wigley, T. Barnett, J. Boyle, W. Brüggemann, N. Gillett, S. Klein, G. Meehl, T. Nozawah, D. Pierce, P. Stott, W. Washington, and M. Wehner (2007). Identification of human-induced changes in atmospheric moisture content, *Supporting Information: SI Table 2*. *PNAS 104*, 15248–15253, doi:10.1073/pnas.0702872104.

Stern, D. I. (2005). Global sulfur emissions from 1850 to 2000. *Chemosphere 58*, 163–175.

Wallace, J. and P. Hobbs (2006). *Atmospheric Science* (Second ed.), Volume 92 of *International Geophysics Series*, pp. 390, 451. Academic Press.

Wikipedia (2009). Beer-lambert law in the atmosphere. *http://en.wikipedia.org/wiki/Beer-Lambert* (accessed April 2009).